RESEARCH ARTICLE

Finite Time Adaptive SMC for UAV Trajectory Tracking Under Unknown Disturbances and Actuators Constraints

KHELIL SIDI BRAHIM[1,2]**, AHMED EL HAJJAJI**[2]**, NADJIBA TERKI**[3]**, AND DAVID LARA ALABAZARES**[4]

[1]Department of Electrical Engineering, LMSE Laboratory, University of Biskra, Biskra 07000, Algeria
[2]Modeling, Information and Systems Laboratory, University of Picardie Jules Verne, 80000 Amiens, France
[3]Department of Electrical Engineering, LESIA Laboratory, University of Biskra, Biskra 07000, Algeria
[4]Postgraduate Department, Higher Technological Institute of Misantla, National Technological Institute of Mexico, Misantla 92830, Mexico

Corresponding author: Khelil Sidi Brahim (khelil.sidibrahim@u-picardie.fr)

ABSTRACT This paper deals with the quadrotor craft trajectory tracking problem subject to unknown disturbance and actuator constraints. A new adaptive sliding mode control (ASMC) with finite-time convergence characteristics is proposed to guarantee quadrotor hovering in spite of parametric uncertainties and external disturbances. Compared with conventional sliding mode controller (SMC), the proposed adaptive algorithm has been developed for the vehicle altitude and attitude control, with unknown bounded of lumped uncertainties. This approach is based on a dynamical adaptive control law to avoid the overestimation and to ensure the convergence in a finite time. In addition, to solve the actuator saturation problem an auxiliary system is used. Stability analysis is demonstrated via Lyapunov theory, exhibiting that the proposed control strategy ensures that all signals of the closed-loop system are bounded and that the tracking errors are bounded in finite time. Numerical simulations and experimental results are given to illustrate the effectiveness of the proposed method, in which a comparative study with conventional SMC found in literature has been made. Experimental validation of the control strategy is carried-out using the parrot mambo mini-UAV.

INDEX TERMS Adaptive sliding mode control, input saturation constraints, trajectory tracking.

I. INTRODUCTION

Unmanned aerial vehicles (UAVs) have attracted vast attention due to their use in numerous civil and military tasks such as strategic reconnaissance operations, crop spraying, weed detection, photography, etc. Among the different types of UAVs, the quadrotor is the most used in the field of automatic control due to its great maneuverability and its thrust to weight ratio, that is better than other's configurations. In addition, the quadrotor achieves a stable hover, balancing the propulsion impulse generated by the four rotors. Unlike

the ordinary helicopter with its complicated mechanism, a quadrotor has a simple mechanical configuration that allows it to achieve the six degrees of freedom motion, driven only by four rotors placed symmetrically with respect to its small center of mass [1]. Despite the advantages of this vehicle in its applications, the design of its flight control system remains a challenge due to its nonlinear dynamics, limitations of its actuators and the presence of disturbances and parametric uncertainties.

A. RELATED WORK ON UAV TRACKING CONTROL

Many control techniques have been developed for quadrotor helicopters, among which we could name:

The associate editor coordinating the review of this manuscript and approving it for publication was Mouquan Shen.

1) LINEAR CONTROLLERS

PID control is one of the preferred algorithms to stabilize the quadrotor, for example in [2] the concepts of feed-forward inverse actuator model and the input space redefinition are explored to extend the performance operating range of a PID flight controller. LQR approaches are used to design optimal tracking controllers for UAVS, for instance in [3] a controller for an unmanned autonomous helicopter slung-load system under external disturbance is proposed, where the model is obtained by using the small perturbation linearization method, considering parametric uncertainty and disturbance. A fractional-order ($PI^\lambda D$) is proposed in [4]. The H_∞ control has been used to improve flight stabilization under external disturbances in [5]. These techniques are limited in their effectiveness when applied beyond the operational point, as their success is not guaranteed.

2) NONLINEAR CONTROLLERS

The most commonly used nonlinear control algorithms for trajectory tracking of UAV are the backstepping based controllers, for instance [6] and [7], and SMC, appearing in [8], [9], and [10]. The disadvantages of backstepping include low robustness to uncertainties and disturbances, as well as the problem of complexity explosion due to repetitive derivations of the virtual control function. The major inconvenience of SMC is the chattering phenomenon in the control signals caused by the discontinuity of this control law. In this context many works have been conducted on the adaptive control as in [11] and [12]. The major drawback of these approaches is the use of intelligent artificial techniques such as neural networks and fuzzy logic, which considerably increases the computational cost and complexity of the implementation. To avoid the previous mentioned disadvantages, a more simple and powerful adaptive law is proposed and developed, which has the ability to improve control accuracy and reduce chattering phenomena.

3) FINITE TIME CONTROL

Finite time control has gained popularity in recent years due to its numerous benefits over classical control approaches, such as fast transient response, robustness to external disturbances and uncertainties, and the ability to achieve control objectives in a limited time frame. For instance, in [13], [14], and [15] authors have studied the finite-time trajectory tracking for quadrotor, in [16] a similar study was conducted for an amphibious robot, while in [17] it was carried out for a reentry vehicle. More recently, a fractional order terminal sliding mode control that allows the convergence of quadrotor trajectories in finite time has been proposed in [18]. In [19], an adaptive command-filtered backstepping SMC has been proposed for finite-time tracking in the presence of uncertainties and disturbances with an unknown upper bound.

Each one of the previously mentioned studies has its own advantages. However, when designing a robust nonlinear controller, it is crucial to consider the amplitude of the control signal in order to prevent actuators from saturating, which is a constraint on the input signal caused by physical limitations of the actuator devices. Input saturation can cause large overshoots, reducing the control performance accuracy, and degrades the system stability. Several works have addressed this problem, to mention, a robust adaptive controller with an auxiliary system for Diesel engine air path proposed in [20], a finite time tracking controller for a quadrotor with input saturation developed in [21], and an anti-windup compensator for a quadrotor designed in [22]. In [23], a cascade saturation controller has been considered for the outer control system, while a classical PID was used for the inner loop control. However, as the input saturation constraints are related to the limitations of the actuators, proof of concept requires extensive and deep experimental tests, which are often missing in these studies. Therefore, in addition to theoretical, simulation, and comparison studies, our work includes an experimental investigation of the proposed control technique on the Parrot Mambo mini-UAV.

SMC has been widely used as an effective control method for systems with uncertainties, ensuring convergence in finite time [24]. This has made it a popular choice for quadrotor trajectory tracking, as is demonstrated in [10] and [25]. Research has also focused on high-order SMC algorithms, such as those presented in [26] and [27]. Additionally, the combination of SMC with artificial intelligence techniques has been explored in works like [28], [29], [30]. Despite of the advantages offered by SMC, such as finite time convergence and good performance, the proposed technique requires knowledge of the upper bound of perturbations, which is often unknown or not constant in practice. As a result, SMC gains may be overestimated, leading to undesirable chattering effects, which is a challenge when the SMC is implemented.

In light of the drawbacks associated with the conventional SMC, as described in the preceding paragraph, a significant number of researchers have directed their efforts towards developing solutions to address these issues. Inspired by the work of [31], a new adaptive gain law for discontinuous control is proposed. This technique allows to obtain a dynamic adaptation of the gains with the smallest possible values but sufficient to reject the external disturbances, ensuring the sliding mode. Among the adaptive laws developed in the literature, the main ones are studied in [32] and [33], where the authors proposed an approach based on a monotonic gain increase until reaching the steady state. However, this technique is less robust and may lead to an overestimation of gains. An adaptation law based on the use of an equivalent control value has been proposed in [34] and [35], nevertheless, the filter requires the knowledge of the first derivative upper bound of disturbances. In [36] and [37], researchers have proposed an approach that uses an increase-decrease gain to address the issues of classical SMC. This method guarantees finite-time convergence, but the convergence time and stability region depend on the disturbance upper bound.

TABLE 1. Comparison of the ASMC features with other approaches.

Related Works	A	B	C	D	E
[38]	No	No	No	Yes	No
[39]	No	No	No	Yes	Yes
[40]	No	No	No	Yes	Yes
[28]	No	No	Yes	Yes	No
[41]	No	No	Yes	No	Yes
[17]	No	Yes	No	Yes	No
[16]	No	Yes	No	Yes	No
[42]	Yes	Yes	No	Yes	No
[43]	No	No	No	Yes	No
[44]	No	Yes	Yes	No	No
[45]	No	Yes	Yes	No	No
[46]	No	Yes	Yes	No	Yes
[47]	No	No	Yes	No	No
[48]	No	Yes	Yes	No	No
[49]	No	Yes	Yes	No	No
[50]	No	No	No	Yes	No
[13]	Yes	No	No	Yes	No
[19]	Yes	No	Yes	Yes	No

B. PROPOSED METHODOLOGY AND CONTRIBUTIONS

Given the problems mentioned above, the challenge is to design an ASMC for altitude and attitude tracking control of a quadrotor, which can prevent the input signal to exceed the saturation limits, while maintaining the desired performance specifications such as finite time convergence, less computational effort for real time implementation, and handle non-linearities and uncertainties without a priory knowledge of the perturbations bounds. Then, main features and contributions of the proposed approach are summarized as follows:

A ASMC that does not require information a priory about the bounds of disturbances

B The ASMC law can adjust the gains without overestimating its value.

C An auxiliary system into the control scheme deal with the actuators saturation, providing good adaptation through a reasonable input signal, with less effort, suitable to practical applications.

D The proposed control strategy guarantees the finite-time stability of the closed-loop system, even under actuator constraints.

E Real-time experimental validation of the theoretical study on a Parrot mambo mini-drone.

To clarify the effectiveness of the proposed ASMC, a comparison with other related works with respect to the features listed above is summarised in Table 1.

The rest of the paper is organized as follows: In Section II, we introduce the altitude and attitude quadrotor model. Section III presents the ASMC design and the Lyapunov stability analysis. The simulation and experimental results are presented in Section IV. Finally, the conclusion is given in Section V.
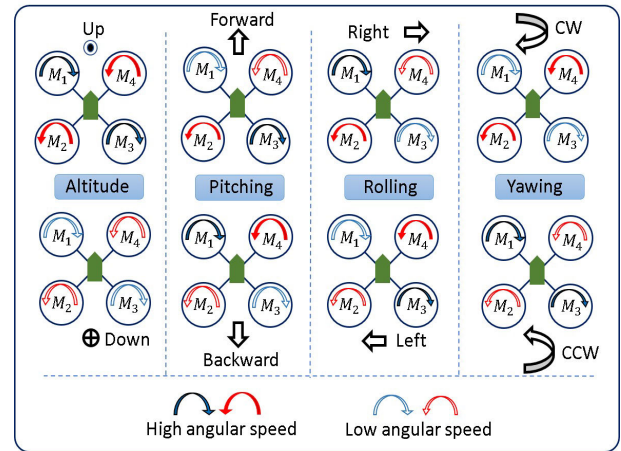

FIGURE 1. Movements in function of ω for the $\times$ configuration.

II. QUADROTOR MODELING

A. QUADROTOR CONFIGURATIONS

Quadrotor structure is simple enough, it comprises of four electrical rotors, attached at the arms ends of a symmetric frame in cross form, which generate the main forces and moments acting on the quadrotor. According to the position of the rotors, with respect to $x - y$ axis of the body reference frame F_b, there are two quadrotor configurations: The plus (+) and cross ($\times$) configurations. In the first, the most common in the literature, the arms are aligned along the $x - y$ axes in F_b. In the second, the perpendicular cross arms are rotated 45° with respect to the $x - y$ axes in F_b. With a better angle of view, the ($\times$) configuration is suitable to install a front camera. The advantage of ($\times$) with respect (+) configuration, is that for the same desired motion, the cross-frame structure provides a higher momentum, increasing the maneuverability performance due that all rotors vary their speed. However, the altitude and yaw control are the same, while the roll and pitch control are basically analogous [51]. Vehicle movement depends directly on the interaction of each rotors as can be seen graphically in Fig. 1, where rotors are denoted by $M_r, r = 1, 2, 3, 4$. The pair M_1 and M_3 rotates clockwise (CW) while the pairs M_2 and M_4, rotates counter-clockwise (CCW), reducing to small values the gyroscopic effects and the aerodynamic torques in stationary trimmed flight. The rotor angular speed is denoted as $\omega_{M_r}, r = 1, \ldots, 4$.

The movement strategy for the $\times$-style quadrotor configuration based on ω_{M_r} values is presented in Table 2. The corresponding movements for each case are determined by the calculated value as follows:

- Altitude: $value = (\omega_{M_1} + \omega_{M_2} + \omega_{M_3} + \omega_{M_4}) - \omega_o$
- Pitching: $value = (\omega_{M_2} + \omega_{M_3}) - (\omega_{M_1} + \omega_{M_4})$
- Rolling: $value = (\omega_{M_1} + \omega_{M_2}) - (\omega_{M_3} + \omega_{M_4})$
- Yawing: $value = (\omega_{M_2} + \omega_{M_4}) - (\omega_{M_1} + \omega_{M_3})$

Note that the total thrust must be constant, during the pitching, rolling and yawing moment to keep the desired altitude.

TABLE 2. Quadrotor movement strategy in function of ω_{M_r}.

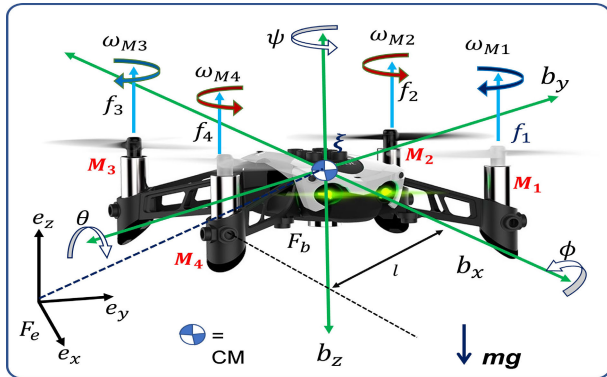| value	Altitude	Pitching	Rolling	Yawing
> 0	Up	Forward	Right	CW
$= 0$	Z_{ref}	Hover	Hover	No Turn
< 0	Down	Backward	Left	CCW

FIGURE 2. Schema of forces and moments acting on the quadrotor helicopter.

B. DYNAMIC MODEL

The quadrotor used here, shown in Fig. 2, is the mambo Parrot drone toy, which has ($\times$) configuration, with good maneuver, able to hover in air fixed point, and can takeoff and land vertically (VTOL). In the *free body scheme* of forces and moments we can see that the forces are denoted as f_r, $r = 1, .., 4$, the inertial and body reference frames are represented by $F_e = \{e_x, e_y, e_z\}$ and $F_b = \{b_x, b_y, b_z\}$, respectively, and the mass center is denoted by CM.

To obtain the attitude equations the Vehicle Flat-Earth model from [52] is used, which have five equations to represent the rotation, position, kinematics, forces and moments as follows:

$$C_{b/n} = fn(\Phi) \tag{1a}$$

$$^e\dot{\mathbf{p}}^n_{CM/T} = C_{n/b}\mathbf{v}^b_{CM/e} \tag{1b}$$

$$\dot{\Phi} = H(\Phi)\,\omega^b_{b/e} \tag{1c}$$

$$^b\dot{\mathbf{v}}^b_{CM/e} = \frac{\mathbf{F}^b_{A,T}}{m} + C_{b/n}\mathbf{g}^n - \Omega^b_{b/e}\mathbf{v}^b_{CM/e} \tag{1d}$$

$$^b\dot{\omega}^b_{b/e} = \left(I^b\right)^{-1}\left[\mathbf{M}^b_{A,T,G} - \Omega^b_{b/e}I^b\omega^b_{b/e}\right] \tag{1e}$$

where, $C_{b/n} \in SO(3) : F_e \rightarrow F_b$, is a orthogonal rotation matrix, $F^b_{A,T} \in F_b$, is the aerodynamic and thrust force vector, $\omega^b_{b/e} = [P\ Q\ R]^T \in F_b$ and $\dot{\Phi} = [\dot{\phi}\ \dot{\theta}\ \dot{\psi}]^T \in F_e$ are angular velocities vectors, $\Omega^b_{b/e} = (\omega^b_{b/e}\times)$, $^e\mathbf{p}^n_{CM/T}$ is the CM position with respect to F_e origin, and $\mathbf{v}^b_{CM/e} \in F_b$ is the velocity vector, with CM and F_b origin coincident.

The kinematic equation (1c) is combined with (1e) to obtain the attitude subsystem, where the term $H(\Phi)$ represents the transformation of the angular velocity components generated by an Euler rotation sequence from F_b to F_e, and is written as (4.4.7) in [53]. Then, considering the vehicle

evolves performing angular motions of low magnitude, from (1c), we have that $[\dot{\phi}\ \dot{\theta}\ \dot{\psi}]^T = [P\ Q\ R]^T$. Equation (1e) is the second Newton law for the angular movement, where $M^b_{A,T,G} = [\ell\ m\ n]^T$ is the total rolling (ℓ), pitching (m) and yawing (n) moments. which is calculated as the algebraic sum of the thrust (M_T), aerodynamics (M_A) and gyroscopic (M_G) moments, as $M^b_{A,T,G} = M_T - M_A - M_G$. The moment M_T is produced by the lift ($F_i = k_t\omega^2_{Mi}$) and drag ($D_i = k_d\omega^2_{Mi}$) forces generated at each rotor shaft, located at distance l from the CM. The constants k_t and k_d are the propeller thrust and drag coefficients. $M_A = K_{fai}\omega^2$, $i = x, y, z$ is the effect of the friction generated by the propeller rotation and the structure frame movement. M_G appears when the vehicle rotates around its CM with rotors turning at high speed, whose axes are parallel to the vehicle z axis, then using J_r to denote the inertia of each rotor, the individual gyroscopic moment vector for each rotor is $\tau_{gi} = \Omega^b_{b/e}J_r[0\ 0\ \omega_{Mi}]^T$ and the total gyroscopic moment can be calculated as the sum of these individual moments $M_G = \sum_{i=1}^{4}(-1)^{i+1}\tau_{gi}$. Then, using these definitions, the total moment can be expressed in the following way:

$$M^b_{A,T,G} = \begin{bmatrix} lk_tW_\phi \\ lk_tW_\theta \\ lk_dW_\psi \end{bmatrix} - \begin{bmatrix} K_{fax}P^2 \\ K_{fay}Q^2 \\ K_{faz}R^2 \end{bmatrix} - J_r \begin{bmatrix} Q \\ -P \\ 0 \end{bmatrix} \left[\overline{W}\right] \tag{2}$$

where $\overline{W} = \omega_{M_1} - \omega_{M_2} + \omega_{M_3} - \omega_{M_4}$, $W_\phi = \omega^2_{M_1} + \omega^2_{M_2} - \omega^2_{M_3} - \omega^2_{M_4}$, $W_\theta = -\omega^2_{M_1} + \omega^2_{M_2} + \omega^2_{M_3} - \omega^2_{M_4}$ and $W_\psi = \omega^2_{M_1} - \omega^2_{M_2} + \omega^2_{M_3} - \omega^2_{M_4}$.

Assuming that the vehicle has symmetry with respect to the xz and yz planes in F_b, then, the inertia matrix is symmetric, $I^b = \{I^b_{i,j}|diag(I^b) = \{I_x, I_y, I_z\}, \forall\ i = j, I^b_{i,j} = 0\ \forall\ i \neq j,\ i, j = 1, 2, 3\}$, whose inverse $(I^b)^{-1}$ has similar characteristics with $diag((I^b)^{-1}) = \{1/I_x, 1/I_y, 1/I_z\}$. Then, using these matrices and the moment vector (2) in (1e) yields:

$$\ddot{\phi} = \frac{1}{I_x}\left[(I_y - I_z)\dot{\theta}\dot{\psi} - K_{fax}\dot{\phi}^2 - J_r\dot{\theta}\overline{W} + lu_\phi\right] \tag{3a}$$

$$\ddot{\theta} = \frac{1}{I_y}\left[(I_z - I_x)\dot{\psi}\dot{\phi} - K_{fay}\dot{\theta}^2 + J_r\dot{\phi}\overline{W} + lu_\theta\right] \tag{3b}$$

$$\ddot{\psi} = \frac{1}{I_z}\left[(I_x - I_y)\dot{\theta}\dot{\phi} - K_{fay}\dot{\psi}^2 + lu_\psi\right] \tag{3c}$$

where the system control inputs are $u_k, k = \{z, \phi, \theta.\psi\}$ which are written in function of the angular velocities of the rotors as follows:

$$\begin{bmatrix} u_z \\ u_\phi \\ u_\theta \\ u_\psi \end{bmatrix} = \begin{bmatrix} k_t & k_t & k_t & k_t \\ k_t & k_t & -k_t & -k_t \\ -k_t & k_t & k_t & -k_t \\ k_d & -k_d & k_d & -k_d \end{bmatrix} \begin{bmatrix} \omega^2_{M1} \\ \omega^2_{M2} \\ \omega^2_{M3} \\ \omega^2_{M4} \end{bmatrix} \tag{4}$$

Then, the altitude and attitude dynamic model (3) of the quadrotor can be written as follows:

$$\ddot{z} = -g + \frac{cos(\theta)cos(\phi)}{m} u_z \tag{5a}$$

$$\ddot{\phi} = \frac{I_y - I_z}{I_x} \dot{\theta}\dot{\psi} - \frac{K_{fax}}{I_x}\dot{\phi}^2 - \frac{J_r}{I_x}\dot{\theta}\overline{W} + \frac{l}{I_x}u_\phi \tag{5b}$$

$$\ddot{\theta} = \frac{I_z - I_x}{I_y} \dot{\psi}\dot{\phi} - \frac{K_{fay}}{I_y}\dot{\theta}^2 + \frac{J_r}{I_y}\dot{\phi}\overline{W} + \frac{l}{I_y}u_\theta \tag{5c}$$

$$\ddot{\psi} = \frac{I_x - I_y}{I_z} \dot{\theta}\dot{\phi} - \frac{K_{fay}}{I_z}\dot{\psi}^2 + \frac{l}{I_z}u_\psi \tag{5d}$$

For physical reasons, the roll, pitch and yaw angles satisfy the following inequalities $-\frac{\pi}{2} < \phi < \frac{\pi}{2}$, $-\frac{\pi}{2} < \theta < \frac{\pi}{2}$ and $-\pi < \psi < \pi$.

III. PROBLEM FORMULATION AND PRELIMINARIES

From the dynamic model (5), the quadrotor altitude and attitude systems can be formulated as follows:

$$\begin{cases} \dot{\chi}_{1i} &= \chi_{2i}, \\ \dot{\chi}_{2i} &= f_i(\chi) + \Delta f_i(\chi) + (b_i(\chi) + \Delta b_i(\chi))u_{si} \\ &\quad + d_i(t), \\ y_i &= \chi_{1i}, i \in \{z, \phi, \theta, \psi\}. \end{cases} \tag{6}$$

where $\chi = [\chi_{1z}, \chi_{2z}, \chi_{1\phi}, \chi_{2\phi}, \chi_{1\theta}, \chi_{2\theta}, \chi_{1\psi}, \chi_{2\psi}]^T = [z, \dot{z}, \phi, \dot{\phi}, \theta, \dot{\theta}, \psi, \dot{\psi}]^T$ is the system state vector, y_i is the system output, $f_i(\chi)$ is the nominal nonlinear dynamic function and $b_i(\chi)$ is the input control function, which are defined as $f_z(\chi) = -g, f_\phi(\chi) = \frac{I_y - I_z}{I_x}\chi_{2\theta}\chi_{2\psi} - \frac{K_{fax}}{I_x}\chi_{2\phi}^2 - \frac{J_r}{I_x}\chi_{2\theta}\overline{W}$, $f_\theta(\chi) = \frac{I_z - I_x}{I_y}\chi_{2\phi}\chi_{2\psi} - \frac{K_{fay}}{I_y}\chi_{2\theta}^2 + \frac{J_r}{I_y}\chi_{2\phi}\overline{W}$, $f_\psi(\chi) = \frac{I_x - I_y}{I_z}\chi_{2\theta}\chi_{2\phi} - \frac{K_{fay}}{I_z}\chi_{2\psi}^2$, $b_z(\chi) = \frac{cos(\theta)cos(\phi)}{m}$, $b_\phi(\chi) = \frac{1}{I_x}$, $b_\theta(\chi) = \frac{1}{I_y}$, $b_\psi(\chi) = \frac{1}{I_z}$, and $d_i(t)$ is unknown external disturbance function that is added to the quadrotor model considering the nonlinearities effects like wind external forces, $\Delta f_i(\chi)$ and $\Delta b_i(\chi)$ are the uncertainties of the dynamic functions and the uncertainties of input control functions, respectively.

According to (4), the control input u_{si} depends on the bounded rotors speed ω_{M_i}, this due to their physical construction limit. Therefore, the input signal must be bounded in a reasonable range $u_{si} \in [-u_i^{max}, u_i^{max}]$ relying on the characteristics of the motor. In other words, the saturation constraint $u_{si} = sat(u_i)$ can be written as follows:

$$u_{si} = \begin{cases} u_i^{max} & if \ u_i \geq u_i^{max} \\ u_i & if -u_i^{max} \leq u_i \leq u_i^{max} \\ -u_i^{max} & if \ u_i \leq -u_i^{max} \end{cases} \tag{7}$$

where u_i^{max} is the absolute maximum value. Using a smooth hyperbolic function, one can approximate the non-smooth saturation function for the sake of improving the smoothness of control signal and avoiding the sharp corner as shown in [54, eq. (7)] (see Fig. 3), which is defined in the following
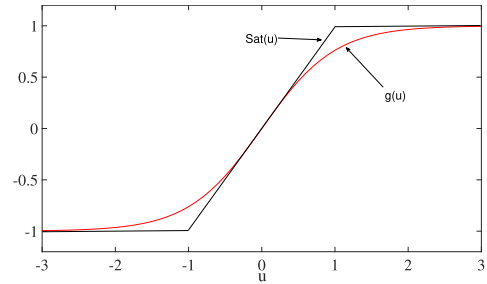

FIGURE 3. Approximation of the saturation function with tanh.

way:

$$g_i(u_i) = (u_i^{max}) \tanh\left(\frac{u_i}{u_i^{max}}\right) \tag{8}$$

where

$$\tanh(u_i/u_i^{max}) = \frac{e^{u_i/u_i^{max}} - e^{-u_i/u_i^{max}}}{e^{u_i/u_i^{max}} + e^{-u_i/u_i^{max}}} \tag{9}$$

then u_{si} in terms of $g_i(u_i)$ can be formulated as $u_{si} = g_i(u_i) + \epsilon_i(u_i)$ or equivalently:

$$u_{si} = (u_i^{max}) \tanh\left(\frac{u_i}{u_i^{max}}\right) + \epsilon_i(u_i) \tag{10}$$

where $\epsilon_i(u_i) = u_{si} - g_i(u_i)$ is a bounded function in time, that is $|\epsilon_i(u_i)| = |u_{si} - g_i(u_i)| \leq u_i^{max}(1 - \tanh(1)) = \varepsilon_i$.

Remark 1: To address non-smooth saturation in control systems, some authors [55], [56] have proposed using a hyperbolic smooth function. However, determining the upper bound of the approximation error is necessary to ensure system stability. In our study, we developed a stability condition without knowing this bound.

The total nonlinear dynamic functions, including the disturbances expressions, are denoted in the following way:

$$\begin{aligned} h_i(\chi, t) &= d_i(t) + \Delta f_i(\chi) + \Delta b_i(\chi)(g_i(u_i) \\ &\quad + \epsilon_i(u_i)) + b_i(\chi)\epsilon_i(u_i) \end{aligned} \tag{11}$$

Using (11) and after some manipulations, the system (6) can be rewritten as follows:

$$\dot{\chi}_{2i} = f_i(\chi) + b_i(\chi)g_i(u_i) + h_i(\chi, t), \tag{12}$$

This new representation has been written in such way, due that the nonlinear functions and the disturbances of each subsystem are lumped in just one nonlinear function.

Assumption 1: In this representation: a) state vector χ is assumed to be bounded and available for measurement, b) disturbance $d_i(t)$ is bounded by an unknown constant $D_i > 0$, that is $\|d_i(t)\| \leq D_i$, c) uncertain terms $\Delta f_i(\chi)$ and Δb_i are bounded by positive unknown constants, satisfying $\|\Delta f_i(\chi)\| \leq \bar{F}_i$ and $\|\Delta b_i(\chi)\| \leq \bar{B}_i$ and d) functions $h_i(\chi, t)$ are assumed unknown and bounded by unknown constants $\bar{h}_i$ such that the condition $|h_i(\chi, t)| \leq \bar{h}_i$ is satisfied.

This assumption has been largely adopted to design control algorithms, for instance in [21]. The first item is feasible since

most of quadrotor experimental platforms are equipped with sensors, like in our case, in which real-time experiment is performed using the Parrot mambo mini-drone. In addition, it is clear that the function $h_i(\chi, t)$ is bounded since it is a sum of bounded functions.

To proof stability the following lemmas and definitions will be used.

Lemma 1: [57] [Young Inequality] $\forall (x, y) \in R \times R$, the following inequality holds:

$$xy \leq \frac{\varepsilon^a}{a}|x|^a + \frac{1}{b\varepsilon^b}|y|^b \tag{13}$$

where $\varepsilon > 0, a > 1, b > 1$ and $(a-1)(b-1) = 1$.

Lemma 2: [58] For any $x_i \in R$ with $i = 1, \ldots, n$ and $0 < \epsilon \leq 1$, then $(|x_1| + |x_2| + \cdots |x_n|)^\epsilon \leq |x_1|^\epsilon + |x_2|^\epsilon + \cdots |x_n|^\epsilon$.

Lemma 3: [59]: For any nonlinear system $\dot{x} = f(x)$, $f(0) = 0, x \in \Re^n$. Suppose that there exists a Lyapunov function V (x) such that $\dot{V}(x) + \eta_1 V^\mu(x) \leq 0$ with scalars $\eta_1 > 0$ and $\mu \in (0, 1)$. Then the origin is a finite-time stable equilibrium point, with settling time $t_f \leq \frac{2}{\eta_1}V_1(t_0)^\mu$.

Lemma 4: [60]: For any Lyapunov function that verifies the following inequality $\dot{V}(x) + \lambda_1 V(x) + \lambda_2 V^\gamma(x) \leq 0$, where $\lambda_1 > 0, \lambda_2 > 0, 0 < \gamma < 1$ are scalars, there exists a finite time stability where the settling time is given by

$$t_f \leq t_0 + \frac{1}{\lambda_1(1-\gamma)} \ln \frac{\lambda_1 V^{1-\gamma}(t_0) + \lambda_2}{\lambda_2} \tag{14}$$

Lemma 5: [61]: Consider system $\dot{x} = f(x)$. Suppose $V(x)$ Lyapunov function with $V(0) = 0$, real numbers $\beta_1, \beta_2 > 0, 0 < p < 1$ and $0 < \delta < \infty$ such that $\dot{V}(x) \leqslant -\beta_1 V(x) - \beta_2 V^p(x) + \delta$, then the trajectory of $\dot{x} = f(x)$ is practical finite-time stable (*PFS*) and the residual set of the solution of system is given by

$$\Delta = \min \left\{ \frac{\delta}{(1-\gamma)\beta_1}, \left(\frac{\delta}{(1-\gamma)\beta_2}\right)^{\frac{1}{p}} \right\} \tag{15}$$

where $0 < \gamma < 1$. The settling time is given as:

$$T \leqslant \max \left\{ \frac{1}{\gamma\beta_1(1-p)} \ln \frac{\gamma\beta_1 V^{1-p}(x_0) + \beta_2}{\beta_2}, \right.$$
$$\left. \frac{1}{\beta_1(1-p)} \ln \frac{\beta_1 V^{1-p}(x_0) + \gamma\beta_2}{\gamma\beta_2} \right\} \tag{16}$$

Definition 1 (GUUB): [62] System $\dot{x}(t) = f(x(t), t)$ is global uniformly ultimately bounded (GUUB) if there exist a positive constant a_2, and for every $a_1 > 0$, there is a positive constant $T_c = T_c(a, b)$ such that $\|x(t_0)\|_2 < a_1 \Rightarrow \|x(t)\|_2 \leq a_2, \forall t \geq t_0 + T_c$, where $\|x(t)\|_2 := x^T(t)x(t)$.

Our target is to design an adaptive sliding mode controller (ASMC) for the altitude and attitude quadrotor under a lumped disturbance and actuator constraints. In this manner, all the signals in the closed-loop system must be bounded and the local states $\chi_i = [\chi_{1i}, \chi_{2i}]^T$ track the desired local paths $\chi_i^d = [\chi_{1i}^d, \chi_{2i}^d]^T$ in a finite time, which are assumed analytic.
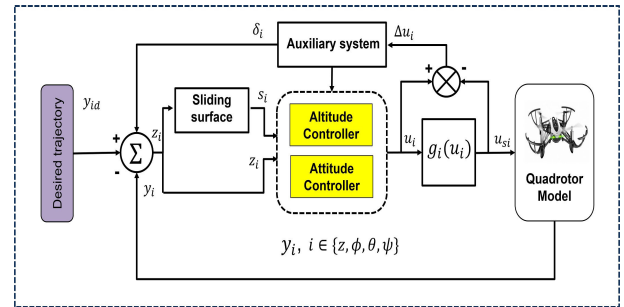

FIGURE 4. Structure control of auxiliary system based SMC.

IV. CONTROLLER DESIGN
In this section, the control design procedure to accomplish a desired trajectory tracking for the vehicle in the presence of uncertainties, external perturbations with unknown bounded and saturation constraints on the actuators is proposed using a constrained ASMC including. The block diagram is shown in Fig. 4.

A. AUXILIARY SYSTEM
The use of an auxiliary system is among the effective and practical control methods, one choice to solve the problem of input saturation [63], the main idea is to introduce a dynamic system that directly deals with the error created by the input saturation limits, i.e., the difference between the value of the control signal and the maximum value reached by the actuator. In this way, the auxiliary system can reduce and compensate the effect of the input saturation. Then, the following auxiliary system is introduced here:

$$\ddot{\delta}_i = -\beta_i'\dot{\delta}_i - \alpha_i\beta_i\delta_i - b_i(\chi)\Delta u_i \tag{17}$$

where δ_i is the auxiliary system variable, α_i and β_i are positive constants and $\beta_i' = \alpha_i + \beta_i$. The auxiliary dynamic system (17) in state form can be written as:

$$\dot{\delta}_{1i} = \delta_{2i} - \alpha_i\delta_{1i} \tag{18}$$
$$\dot{\delta}_{2i} = -\beta_i\delta_{2i} - b_i(\chi)\Delta u_i \tag{19}$$

where $\Delta u_i = u_i - g_i(u_i)$, is the difference between the saturated input signal and the real input signal assumed to be bounded i.e., $|\Delta u_i| \leq \overline{\Delta u_i}$.

The auxiliary system has the same order for each subsystem with Δu_i as an input. It is clear that this auxiliary system has no effect in case the control signal does not reach its limits (i.e. $\Delta u_i = 0$). However, in the other case ($\Delta u_i \neq 0$) it performs as a filter to ensure the error converge to zero. Since the controllability of the system must be satisfied, error Δu_i cannot be large, when the control input is saturated. Therefore, we can conclude that the difference Δu_i is limited.

Theorem 1: Considering auxiliary system (19) under assumption 1, and there exists α_i that satisfies $\alpha_i > \frac{1}{2}$, then the auxiliary system is globally exponentially stable and δ is globally uniformly ultimately bounded (GUUB) if the

inequality $|\delta_{1i}|, |\delta_{2i}| \leq e^{-\frac{1}{2}\gamma_i' t}\sqrt{2V_{\delta_i}(0)}$ holds, where $V_{\delta_i}(0)$ and γ_i' are positive constants.

Proof: Let us define the Lyapunov function as $V_{\delta_i} = \frac{1}{2}\delta_{1i}^2 + \frac{1}{2}\delta_{2i}^2$, whose derivative is calculated in the following way:

$$\dot{V}_{\delta_i} = \delta_{1i}\dot{\delta}_{1i} + \delta_{2i}\dot{\delta}_{2i} \qquad (20)$$

Using the state equation (19) results:

$$\dot{V}_{\delta_i} = \delta_{1i}(\delta_{2i} - \alpha_i\delta_{1i}) + \delta_{2i}(-\beta_i\delta_{2i} - b_i(\chi)\Delta u_i) \qquad (21)$$

regrouping terms we have:

$$\dot{V}_{\delta_i} = \delta_{1i}\delta_{2i} - \alpha_i\delta_{1i}^2 - \beta_i\delta_{2i}^2 - \delta_{2i}b_i(\chi)\Delta u_i \qquad (22)$$

Applying lemma 1, for the first and last term of the right hand side of (22) we obtain:

$$\dot{V}_{\delta_i} \leq -(\alpha_i - \frac{1}{2})\delta_{1i}^2 - \beta_i\delta_{2i}^2 - \frac{1}{2}(b_i(\chi)\overline{\Delta}u_i)^2 \leq 0 \qquad (23)$$

which can also be written as:

$$\dot{V}_{\delta_i} \leq -((\alpha_i - \frac{1}{2})\delta_{1i}^2 + \beta_i\delta_{2i}^2) - \frac{1}{2}(b_i(\chi)\overline{\Delta}u_i)^2 \leq 0 \qquad (24)$$

This inequality can be expressed using the minimum of a set of elements notated in the following way:

$$\dot{V}_{\delta_i} \leq -\min\left\{2(\alpha_i - \frac{1}{2}), 2\beta_i\right\}(\frac{1}{2}\delta_{1i}^2 + \frac{1}{2}\delta_{2i}^2) - \frac{1}{2}(b_i(\chi)\overline{\Delta}u_i)^2 \qquad (25)$$

or

$$\dot{V}_{\delta_i} \leq -\gamma'V_{\delta_i} - \frac{1}{2}(b_i(\chi)\overline{\Delta}u_i)^2 \leq -\gamma_i'V_{\delta_i} \qquad (26)$$

where $\gamma_i' = \min\left\{2(\alpha_i - \frac{1}{2}), 2\beta_i\right\}$. Then, global exponential stability is guaranteed with (22). The solution of the differential inequality (26) is $0 \leq V_{\delta_i} \leq V_{\delta_i}(0)e^{-\gamma' t}$, therefore, from the definition of the Lyapunov function we obtain:

$$|\delta_{1i}|, |\delta_{2i}| \leq e^{-\frac{1}{2}\gamma_i' t}\sqrt{2V_{\delta_i}(0)} \qquad (27)$$

From definition 1 and equation (27), it can be concluded that δ_i is GUUB and Theorem 1 is proved.

B. AUXILIARY SYSTEM-BASED SMC

To combine the sliding mode control with the auxiliary system, a modified tracking error can be defined as $e_i = \chi_{1i} - \chi_{1i}^d - \delta_i$, then, let s_i be the sliding surface given as follows:

$$s_i = \dot{e}_i + \lambda_i e_i \quad \lambda_i > 0 \qquad (28)$$

The time derivative of (28) is:

$$\dot{s}_i = \ddot{e}_i + \lambda_i\dot{e}_i \qquad (29)$$

By substituting (12) and (17) into (29), yields:

$$\dot{s}_i = f_i(\chi) + b_i(\chi)g_i(u_i) + h_i(\chi, t) - \dot{\chi}_{2i}^d + \beta_i'\dot{\delta}_i + \alpha_i\beta_i\delta_i + b_i(\chi)\Delta u_i + \lambda_i\dot{e}_i \qquad (30)$$

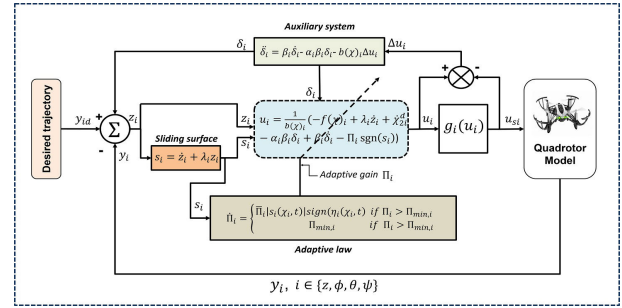**FIGURE 5.** Block diagram of the proposed method.

Now, if the following switching control law is selected:

$$\dot{s}_i = -\Pi_i(t)sign(s_i) + h_i(\chi, t) \qquad (31)$$

then the SMC law based on the auxiliary system is:

$$u_i = \frac{1}{b_i(\chi)}(-f_i(\chi) - \lambda_i\dot{e}_i + \dot{\chi}_{2i}^d - \alpha_i\beta_i\delta_i - \beta_i'\dot{\delta}_i - \Pi_i(t)sign(s_i)) \qquad (32)$$

where $\Pi_i(t)$ is an adaptive parameter which will be defined later.

C. ADAPTIVE SLIDING MODE CONTROL LAW

The performance of SMCs depends on knowing the uncertainty limits of the system which are difficult to know in practice. To overcome the problems associated with unknown limits, a novel adaptive sliding mode control (ASMC) law is proposed, whose scheme is shown in Fig. 5. Let us define an auxiliary variable for constructing an adaptive gain as follows:

$$\eta_i(\chi, t) = |s_i(\chi, t)| - \kappa_i\Pi_i(t), \ i \in \{z, \phi, \theta, \psi\}. \qquad (33)$$

where κ_i is a positive parameter, and the proposed adaptive control gain is defined as:

$$\dot{\Pi}_i = \begin{cases} \bar{\Pi}_i|s_i(\chi, t)| \, \text{sign}(\eta_i(\chi, t)) & \text{if } \Pi_i > \Pi_i^{min} \\ \Pi_i^{min} & \text{if } \Pi_i \leq \Pi_i^{min}. \end{cases} \qquad (34)$$

with $\Pi_i(0) > 0$, $\bar{\Pi}_i > 0$ and $\Pi_i^{min} > 0$ very small. Parameter Π_i^{min} is introduced in order to obtain only positive values for Π_i. In the following, without loss of generality but for the sake of clarity, we assume that $\Pi_i^{min} \leq \Pi_i(t) \leq \Pi_i^{max}$ for all $t > 0$, for the discussion and the proof.

Remark 2: The proposed gain-adaptation law (34) permits the gain $\Pi_i(t)$ to decline (while $\eta_i(\chi, t) < 0$) after sliding mode is achieved with regard to $s_i(\chi, t)$, which implies that there is an upper limit Π_i^{max}. In other words, the gain $\Pi_i(t)$ will be kept at the least value that permits to maintain a given level of accuracy.

D. STABILITY ANALYSIS FOR THE ASMC

The following stability analysis for all system states remains the same and is obtained via the same steps, where the subscript i will be removed to avoid that the proof procedure

become cumbersome, indicating that the proof is extensive to all subsystems.

To guarantee the convergence in a finite time, the following theorem is proposed.

Theorem 2: Considering nonlinear uncertain system (12), with satisfied assumption 1, sliding surface (28) control law (32) with adaptive law (34), there exists a finite time $t_f > 0$ so that the sliding surface converge to zero.

Proof: We can define the following Lyapunov function:

$$V = V_s + V_\Pi = \frac{1}{2}s^2 + \frac{1}{2\Upsilon}(\Pi - \Pi^{max})^2 \quad (35)$$

where Υ is a constant that will be calculate later.

Using (34) the derivative of Lyapunov function V can be calculated in the following way:

$$\dot{V} = s\dot{s} + \frac{1}{\Upsilon}(\Pi - \Pi^{max})\bar{\Pi}|s|\operatorname{sign}(\eta) \quad (36)$$

By substituting (31) into (36), yields:

$$\dot{V} = sh - \Pi s\operatorname{sign}(s) + \frac{1}{\Upsilon}\left(\Pi - \Pi^{max}\right)\bar{\Pi}|s|\operatorname{sign}(\eta) \quad (37)$$

having into account that $s\operatorname{sign}(s) \approx |s|$ and that h is bounded (37) becomes:

$$\dot{V} \leq \bar{h}|s| - \Pi|s| + \frac{1}{\Upsilon}\left(\Pi - \Pi^{max}\right)\bar{\Pi}|s|\operatorname{sign}(\eta) \quad (38)$$

using the add-subtract math artifice we have

$$\dot{V} \leq \bar{h}|s| - \Pi|s| + \Pi^{max}|s| - \Pi^{max}|s|$$
$$+ \frac{1}{\Upsilon}\left(\Pi - \Pi^{max}\right)\bar{\Pi}|s|\operatorname{sign}(\eta) \quad (39)$$

whose terms can be grouped as follows:

$$\dot{V} \leq \left(\Pi - \Pi^{max}\right)(\frac{\bar{\Pi}}{\Upsilon}|s|\operatorname{sign}(\eta) - |s|)$$
$$- (\Pi^{max} - \bar{h})|s| \quad (40)$$

applying again the last artifice results:

$$\dot{V} \leq \left(\Pi - \Pi^{max}\right)(\frac{\bar{\Pi}}{\Upsilon}|s|\operatorname{sign}(\eta) - |s|) - \Gamma_1|s|$$
$$+ \Gamma_2\left|\Pi - \Pi^{max}\right| - \Gamma_2\left|\Pi - \Pi^{max}\right| \quad (41)$$

It exists for always $\Pi^{max} > \bar{h}$ then $\Gamma_1 = \Pi^{max} - \bar{h} > 0$ and $\Gamma_2 > 0$ and one gets

$$\dot{V} \leq -\Gamma_1|s| - \Gamma_2\left|\Pi - \Pi^{max}\right| - \Sigma_1(\chi, t) \quad (42)$$

using the minimum of a set of elements (42) becomes

$$\dot{V} \leq -\min\left\{\Gamma_1\sqrt{2}, \Gamma_2\sqrt{2\Upsilon}\right\}\left(\frac{|s|}{\sqrt{2}}\right.$$
$$\left. + \frac{|\Pi - \Pi^{max}|}{\sqrt{2\Upsilon}}\right) - \Sigma_1(\chi, t) \quad (43)$$

and applying lemma 2 the following inequality results:

$$\dot{V} \leq -\Gamma V^{1/2} - \Sigma_1(\chi, t) \quad (44)$$

where $\Sigma_1(\chi, t) = (\frac{\bar{\Pi}}{\Upsilon}|s(\chi, t)|\operatorname{sign}(\eta(\chi, t)) - |s(\chi, t)| - \Gamma_2)|\Pi - \Pi^{max}|$ and $\Gamma = \sqrt{2}\min\left\{\Gamma_1, \Gamma_2\sqrt{\Upsilon}\right\}$.

In order to conclude the convergence in finite time, one has to study the sign of $\Sigma_1(\chi, t)$, where it is clear that it depends on the sign of $\eta(\chi, t)$, therefore there are two cases to analyze:
Case 1 Suppose that $\eta(\chi, t) > 0$. So $\Sigma_1(\chi, t) > 0$ if

$$\left(\frac{\bar{\Pi}}{\Upsilon}|s(\chi, t)| - |s(\chi, t)| - \Gamma_2\right) > 0 \quad (45)$$

$$|s(\chi, t)|\left(\frac{\bar{\Pi}}{\Upsilon} - 1\right) - \Gamma_2 > 0 \quad (46)$$

After performing some algebraic operations, the following expression is obtained:

$$\Upsilon < \frac{\bar{\Pi}}{1 + \frac{\Gamma_2}{\kappa\Pi^{max}}} \quad (47)$$

From (44), one gets

$$\dot{V} \leq -\Gamma V^{1/2} - \Sigma_1(\chi, t) \leq -\Gamma V^{1/2} \quad (48)$$

So we can choose Υ to satisfy inequality (47). According to finite-time stability of Lemma 3, the system is asymptotically stable as per Lyapunov's stability theory, which ensures the finite time convergence of sliding manifold to zero, one can get the expression of reaching time t_{f1} as:

$$t_{f1} \leq \frac{2}{\Gamma}\sqrt{V(t_0)} \quad (49)$$

Case 2 Suppose that $\eta(\chi, t) < 0$. In this case the function $\Sigma_1(\chi, t)$ can be negative, so from (40):

$$\dot{V} = \left(\Pi - \Pi^{max}\right)\left(\frac{\bar{\Pi}}{\Upsilon}|s|\operatorname{sign}(\eta(\chi, t)) - |s|\right) - \Gamma_1|s| \quad (50)$$

$$\dot{V} = \left|\Pi - \Pi^{max}\right||s|\left(\frac{\bar{\Pi}}{\Upsilon} + 1\right) - \Gamma_1|s| \quad (51)$$

Applying lemma 1 to the last term we have the inequality:

$$\dot{V} \leq \frac{1}{2}\Gamma_3^2|s|^2 + \frac{1}{2}\left(\Pi - \Pi^{max}\right)^2 - \Gamma_1|s| \quad (52)$$

where $\Gamma_3 = (\frac{\bar{\Pi}}{\Upsilon} + 1)$ and using again the math artifice (39) the inequality (52) can be expressed in the following manner:

$$\dot{V} \leq -\Gamma_1|s| + \frac{1}{2}\Gamma_3^2|s|^2 - \frac{1}{2}\left(\Pi - \Pi^{max}\right)^2$$
$$+ \left(\Pi - \Pi^{max}\right)^2 \quad (53)$$

Since $\eta(\chi, t) < 0$ and using (33) we have that $|s| < \kappa\Pi$ or $\frac{|s|}{\kappa} < \Pi$, then subtracting in both sides Π^{max} results

$$\frac{|s|}{\kappa} - \Pi^{max} < \Pi - \Pi^{max} \quad (54)$$

which implies that

$$(\Pi - \Pi^{max})^2 < \left(\frac{|s|}{\kappa} - \Pi^{max}\right)^2 \quad (55)$$

Then, using (53) and (55) it can be established:

$$\dot{V} \leq -\Gamma_1|s| + \frac{1}{2}\Gamma_3^2|s|^2 - \frac{1}{2}\left(\Pi - \Pi^{max}\right)^2$$
$$+ (\frac{|s|}{\kappa} - \Pi^{max})^2 \quad (56)$$

Expanding the last term

$$\dot{V} \leq -\Gamma_1|s| + \frac{1}{2}\Gamma_3^2|s|^2 - \frac{1}{2}(\Pi - \Pi^{max})^2 + \frac{1}{\kappa^2}|s|^2 + (\Pi^{max})^2 - \frac{2}{\kappa}|s|\Pi^{max} \qquad (57)$$

Now, let L_1 and L_2 be two positive constants, which are used in (57) to proceed as in (53) to get:

$$\dot{V} \leq -\Gamma_1|s| - (L_1 - (\frac{1}{2}\Gamma_3^2 + \frac{1}{\kappa^2}))|s|^2$$
$$- \frac{1}{2}(\Pi - \Pi^{max})^2 - L_2|\Pi - \Pi^{max}| + L_1|s|^2$$
$$+ (\Pi^{max})^2 - \frac{2}{\kappa}|s|\Pi^{max} + L_2|\Pi - \Pi^{max}| \qquad (58)$$

Inequality (58) can be expressed in the following manner:

$$\dot{V} \leq -\min\left\{(L_1 - (\frac{\Gamma_3^2}{2} + \frac{1}{\kappa})), \Upsilon\right\}\left[\frac{(\Pi - \Pi^{max})^2}{2\Upsilon}\right.$$
$$+ \left.\frac{|s|^2}{2}\right] - \min\left\{\Gamma_1\sqrt{2}, L_2\sqrt{2\Upsilon}\right\}\left[\frac{|\Pi - \Pi^{max}|}{\sqrt{2\Upsilon}}\right.$$
$$+ \left.\frac{|s|}{\sqrt{2}}\right] - \Sigma_2(\chi, t) \qquad (59)$$

which can be abbreviated as follows:

$$\dot{V} \leq -\Gamma_5 V - \Gamma_4 V^{\frac{1}{2}} - \Sigma_2(\chi, t) \qquad (60)$$

where $\Sigma_2(\chi, t) = L_1|s|^2 + (\Pi^{max})^2 - \frac{2}{\kappa}|s|\Pi^{max} + L_2|\Pi - \Pi^{max}|$, $\Gamma_4 = \min\left\{\Gamma_1\sqrt{2}, L_2\sqrt{2\Upsilon}\right\}$ and $\Gamma_5 = \min\left\{(L_1 - (\frac{\Gamma_3^2}{2} + \frac{1}{\kappa})), \Upsilon\right\}$.

From (60) and *Lemma 4*, the finite time convergence of sliding manifold to zero can be ensured if $\Sigma_2(\chi, t) > 0$, which means:

$$0 < L_1|s|^2 + (\Pi^{max})^2 - \frac{2}{\kappa}|s|\Pi^{max} + L_2|\Pi - \Pi^{max}| \quad (61)$$

by using (55), ($\Pi \leq \Pi^{max}$) and after some calculation we find that $L_1 > (\frac{\Gamma_3^2}{2} + \frac{1}{\kappa})$ and $L_2 > 0$. Then, from (60), one gets

$$\dot{V} \leq -\Gamma_5 V - \Gamma_4 V^{\frac{1}{2}} - \Sigma_2(\chi, t) \leq -\Gamma_5 V - \Gamma_4 V^{\frac{1}{2}} \quad (62)$$

Therefore, the expression of the reaching time t_{f2} is given as:

$$t_{f2} \leq t_0 + \frac{2}{\Gamma_5}\ln\frac{\Gamma_5\sqrt{V(t_0)} + \Gamma_4}{\Gamma_4} \qquad (63)$$

The term t_0 is the initial time and $V(t_0)$ is the value of V at $t = t_0$. Then, it can be concluded that the sliding surface converges to zero in a finite time $t_f \leq max\{t_{f1}, t_{f2}\}$. Hence, it is clear that all signals are bounded in finite time, and the *Theorem* 2 is proved.

Theorem 3: Considering nonlinear uncertain system (12), auxiliary system (17), with satisfied assumption 1, sliding surface (28) control law (32) with adaptive law (34), there exists a finite time T_f so that the sliding surface is bounded in finite time.

Proof: Let define the Lyapunov function $V_a = V + V_\delta$, which can be expressed as follows:

$$V_a = \frac{1}{2}s^2 + \frac{1}{2\Upsilon}(\Pi - \Pi^{max})^2 + \frac{1}{2}\delta_1^2 + \frac{1}{2}\delta_2^2 \qquad (64)$$

whose derivative is given as:

$$\dot{V}_a = \dot{V} + \dot{V}_\delta \qquad (65)$$

To demonstrate theorem 3, there are two cases that must be analyzed, according to the sign of $\eta(\chi, t)$, so *Case 1 $\eta(\chi, t) > 0$*, then from (26), (48) and (65) one can get:

$$\dot{V}_a \leq -\gamma V_\delta - \Gamma V \leq -\gamma V_a + \gamma V - \Gamma V^{\frac{1}{2}} \qquad (66)$$

if the add-subtract math artifice is used, results:

$$\dot{V}_a \leq -\gamma V_a + \gamma V - \Gamma V^{\frac{1}{2}} - \Gamma V_a^{\frac{1}{2}} + \Gamma V_a^{\frac{1}{2}} \qquad (67)$$

Then using (48), last equation can be written as:

$$\dot{V}_a \leq -\gamma V_a - \Gamma V_a^{\frac{1}{2}} + \gamma V + \Gamma V_\delta^{\frac{1}{2}} \qquad (68)$$

and by using *lemma 2* one can obtain:

$$\dot{V}_a \leq -\gamma V_a - \Gamma V_a^{\frac{1}{2}} + \gamma V + \frac{1}{2}\Gamma^2 + \frac{1}{2}V_\delta \qquad (69)$$

Applying Young inequality of *lemma 1* results:

$$\dot{V}_a \leq -\left(\gamma - \max\left\{\gamma, \frac{1}{2}\right\}\right)V_a - \Gamma V_a^{\frac{1}{2}} + \frac{1}{2}\Gamma^2 \qquad (70)$$

If we let $\gamma > \frac{1}{2}$, then we have $\left(\gamma - \max\left\{\gamma, \frac{1}{2}\right\}\right) = 0$, so one can obtain:

$$\dot{V}_a \leq -\Gamma V_a^{\frac{1}{2}} + \frac{1}{2}\Gamma^2 \qquad (71)$$

By selecting a scalar $0 < \Gamma_6 < \Gamma$ we can rewrite $\dot{V}_a$ as:

$$\dot{V}_a \leq -\Gamma_6 V_a^{\frac{1}{2}} - (\Gamma - \Gamma_6)V_a^{\frac{1}{2}} + \frac{1}{2}\Gamma^2 \qquad (72)$$

Introduce a scalar $\Xi = \frac{\frac{1}{2}\Gamma^2}{(\Gamma - \Gamma_6)}$, it can be observed that $\dot{V}_a \leq -\Gamma_6 V_a^{\frac{1}{2}}$ when $V_a(t) > \Xi$ so that

$$\dot{V}_a \leq \max\{V_a(0), \Xi\} \qquad (73)$$

We conclude that V_a converge in finite time $T_{f1} \leq \frac{2}{\Gamma_6}\sqrt{V_a(t_0)}$ and entering inside the ball Ξ. From (64) we have $V_a \geq \frac{1}{2}s^2$. According to [62] there is a global ultimate uniform bound (GUUB) ϱ on s is given by:

$$\varrho = \sqrt{\frac{\Gamma^2}{(\Gamma - \Gamma_6)}} \qquad (74)$$

Remark 3: From equation (74), it is clear that a smaller value of Γ and Γ_6 represents a smaller boundary of the region into which the states will enter in a finite time and remain there.

Case 2 $\eta(\chi, t) < 0$, then, from (26), (62) and (65) one can get:

$$\dot{V}_a \leq -\gamma V_\delta - \Gamma_5 V - \Gamma_4 V^{\frac{1}{2}} \tag{75}$$

$$\dot{V}_a \leq -\min\{\Gamma_5, \gamma\} V_a - \Gamma_4 V^{\frac{1}{2}} \tag{76}$$

that can be expressed as

$$\dot{V}_a \leq -\min\{\Gamma_5, \gamma\} V_a - \Gamma_4 V^{\frac{1}{2}} - \Gamma_4 V_a^{\frac{1}{2}} + \Gamma_4 V_a^{\frac{1}{2}}$$

$$\dot{V}_a \leq -\min\{\Gamma_5, \gamma\} V_a - \Gamma_4 V_a^{\frac{1}{2}} + \Gamma_4 V_\delta^{\frac{1}{2}} \tag{77}$$

By using *lemma* 2, inequality (77) can be expressed as

$$\dot{V}_a \leq -\min\{\Gamma_5, \gamma\} V_a - \Gamma_4 V_a^{\frac{1}{2}} + \frac{1}{2}\Gamma_4^2 + \frac{1}{2} V_\delta$$

$$\dot{V}_a \leq -\Gamma_7 V_a - \Gamma_4 V_a^{\frac{1}{2}} + \frac{1}{2}\Gamma_4^2 \tag{78}$$

where $\Gamma_7 = \min\{1, \Gamma_5, \gamma\}$, and according to lemma 5, Lyapunov function V_a converges in finite time T_{f2} into a disc region with radius r defined as follows:

$$r = \min\left\{\sqrt{\frac{\Gamma_4^2}{(1-\mu)\Gamma_7}}, \sqrt{2}\left(\frac{\frac{1}{2}\Gamma_4^2}{(1-\mu)\Gamma_4}\right)\right\} \tag{79}$$

whose convergence time is given in terms of the following inequality

$$T_{f2} \leq \max\left\{\frac{2}{\mu\Gamma_7} \ln \frac{\mu\Gamma_7\sqrt{V_a(t_0)} + \Gamma_4}{\Gamma_4},\right.$$
$$\left.\frac{2}{\Gamma_7} \ln \frac{\Gamma_7\sqrt{V_a(t_0)} + \mu\Gamma_4}{\mu\Gamma_4}\right\} \tag{80}$$

and $0 < \mu < 1$, its clear that s is bounded. This means that the practical finite time stability is ensured and all signals in the closed-loop system are bounded in finite time, $T_f \leq max\{T_{f1}, T_{f2}\}$, then, *Theorem* 3 is proved.

The radius r from (79) denotes the size of the convergence region for the tracking error, which must be minimized to ensure optimal performance. To make r as small as possible the parameters can be chosen as follows: As the parameter Γ_4 depends of the constant L_2, then, choosing L_2 very small results on a smaller Γ_4 and choosing γ large, a larger Γ_7 is guaranteed. Now, with smaller Γ_4 and larger Γ_7 it can be guarantee the smaller r. Inequality (80) represents the time it takes for the tracking error to enter inside of r, and a larger Γ_4 value leads to a faster convergence rate for the error compensation system. Therefore, choosing the optimal value of Γ_4 is critical for both r and T_{f2}. To determine the optimal values of Γ_4, the other parameters in the equations can be varied firstly and then fixed while observing the system's performance with respect to Γ_4.

Remark 4: The term "practical" in the control field means that perfect zero error tracking is often unattainable in real-world scenarios. Instead, the tracking error is typically limited to a bounded region around zero, which is acceptable for most practical applications. Unlike the works [64], [65], where the finite-time stability concept cannot be employed in practice

due to the disturbed conditions [66], our proposed approach has the advantages of be practical in real time implementation, where the stability analysis demonstrates that the state trajectories converge to a small neighbourhood in finite time in the presence of an unknown disturbance.

Remark 5: In contrast with [67] and [21], that propose backstepping controllers, which require a large number of conditions to choice the gains to get convergence in finite time, the controller developed in this work has less restrictive conditions on the control gains, which significantly reduces the complexity for implementation.

Remark 6: To attain the desired control performance using the proposed controller, it is recommended to follow the suggested criteria for parameter selection.

- Parameter λ plays a crucial role in determining the dynamics response of the state in the sliding function. Increasing λ leads to a higher rate of convergence for the state.
- Parameters α and β of the auxiliary system play a critical role in compensating input saturation, as they determine the speed and level of attenuation eliminating the error. However, it is important to note that higher values of α and β can result in a faster response but may also increase the overshoot resulting in instability.
- Parameter $\bar{\Pi}$ is important for designing an adaptive control system. A larger $\bar{\Pi}$ can improve the adaptive rate and reduce the convergence time of the sliding variable, but selecting an excessively large value can cause overshoot in the control gain and lead to control signal chattering.

V. RESULTS

The effectiveness of the proposed control law is shown in two parts, the first, presents the simulation tests for the altitude and attitude systems of the quadrotor, and the second one concerns the experimental validation of the control law for the altitude system using the mambo parrot mini-drone.

A. SIMULATION RESULTS

SIMULINK/MATLAB software is used to evaluate the effectiveness of the proposed control strategy. In order to demonstrate the superiority of the developed control law ASMC over the existing control techniques, a comparative study is carried out with sliding mode control SMC and control law developed in [13]. The real values of Parrot mambo mini-drone parameters and saturation bounds are summarized in Table 3.

The system initial conditions are $\chi_0 = [0, 0, 0, -0.3]^T$ and proposed desired trajectories are given as follows:

$$\chi_z^d = \begin{cases} 0.5 \text{ m}, & \text{for } 0 \leq t < 10 \text{ sec} \\ 1 \text{ m}, & \text{for } 10 \leq t < 27.5 \text{ sec} \\ 0.6 \text{ m}, & \text{for } 27.5 \leq t < 40 \text{ sec} \\ 0.2 \text{ m}, & \text{for } 40 \leq t < 60 \text{ sec} \end{cases},$$

$$\chi_\phi^d = \begin{cases} 0.5 \text{ rad}, & \text{for } 0 \leq t < 20 \text{ sec} \\ -0.5 \text{ rad}, & \text{for } 20 \leq t < 35 \text{ sec} \\ 0.7 \text{ rad}, & \text{for } 35 \leq t < 60 \text{ sec} \end{cases},$$

TABLE 3. Parameters of the quadrotor.

Parameters	Values	Units
l	0.23	m
m	0.063	kg
J_r	1.02×10^{-7}	kg.m^2
I_x	5.82×10^{-5}	kg.m^2
I_y	7.16×10^{-5}	kg.m^2
I_z	1×10^{-4}	kg.m^2
k_p	4.72×10^{-8}	N.m.s^2
k_d	1.13×10^{-10}	N.m.s^2
u_z^{max}	1.2	N
$u_{\phi,\theta}^{max}$	1×10^{-3}	N.m
u_ψ^{max}	1×10^{-4}	N.m
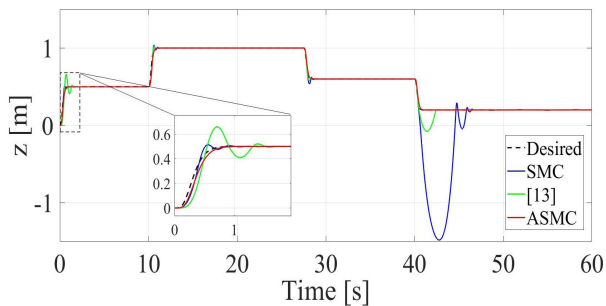
FIGURE 6. Tracking trajectory of altitude.

$$\chi_\theta^d = \begin{cases} -0.5 \text{ rad}, & \text{for } 0 \leq t < 15 \text{ sec} \\ -0.5 \text{ rad}, & \text{for } 15 \leq t < 25 \text{ sec} \\ -0.5 \text{ rad}, & \text{for } 25 \leq t < 40 \text{ sec} \\ 0.7 \text{ rad}, & \text{for } 40 \leq t < 60 \text{ sec} \end{cases},$$

$$\chi_\psi^d = \begin{cases} -0.5 \text{ rad}, & \text{for } 0 \leq t < 15 \text{ sec} \\ 0.7 \text{ rad}, & \text{for } 15 \leq t < 40 \text{ sec} \\ -0.5 \text{ rad}, & \text{for } 40 \leq t < 60 \text{ sec} \end{cases}.$$

Uncertainties and external disturbances are defined as:

- Parametric uncertainties are considered as $\Delta I_i = 0.5 I_i$ for $i \in \{x, y, z\}$.
- External disturbances are assumed to be the effect of wind as $d_i(t) = 0.7 \sin(0.5t)$ for $i \in \{\phi, \theta, \psi\}$ and $d_i(t) = 0.7 \sin(t)$ for $i \in \{z\}$.

Figs (6-9) illustrate the comparison of trajectory tracking. It can be noticed that the proposed method exhibits better tracking performance than other controllers, despite of the presence of external disturbances, uncertainties, and input saturation. In addition, it can be seen that the proposed ASMC exhibits more accurate tracking, eliminates overshoot, and improves transient performance. It can be observed that classical SMC and the controller proposed in [13] show overshoot due to the limitations of the quadrotor actuators that are not accounted by these control methods.

The control input signals are shown in Figs (10-13). The control signal of SMC and control law proposed in [13] require more energy to achieve the target, Additionally, it is evident that the chattering phenomenon exists in [13], which is caused by the control adaptation law. On the other hand, the control signals generated by the ASMC can be smooth
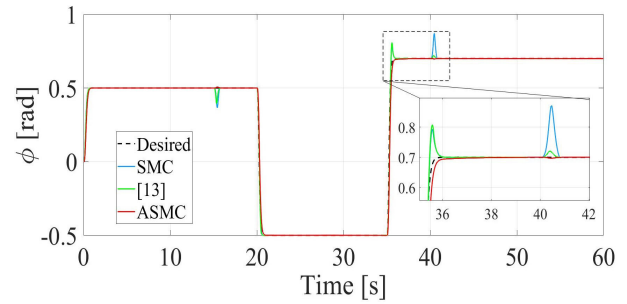

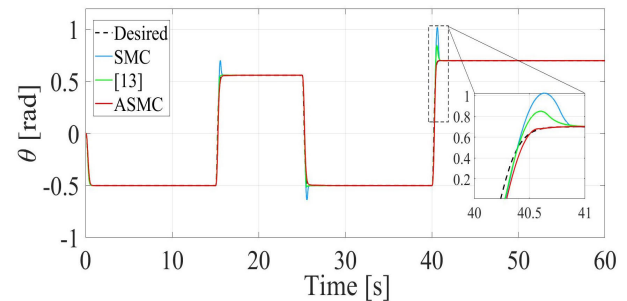**FIGURE 7. Tracking trajectory of roll angle.**
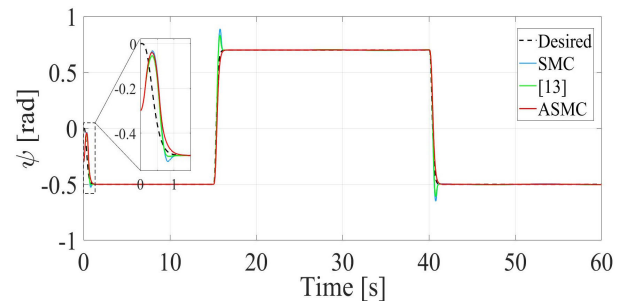

FIGURE 8. Tracking trajectory of pitch angle.

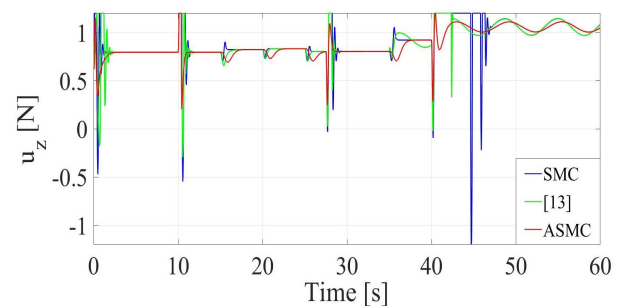**FIGURE 9. Tracking trajectory of yaw angle.**

FIGURE 10. Control input signal u_ψ.

enough to be acceptable under input saturation, then, the convergence can be achieved with less effort.

These Results demonstrates that ASMC guarantees a high tracking performance and handles input saturation. Figs (14-17) evidences the evolution of the adaptation law
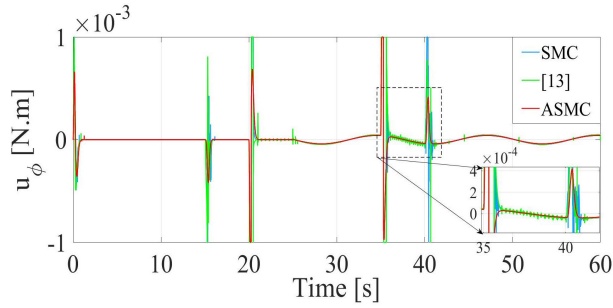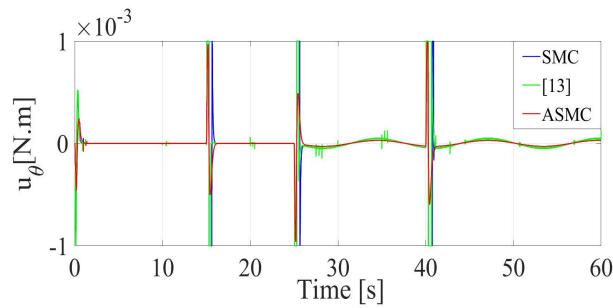
FIGURE 11. Control input signal u_ϕ.
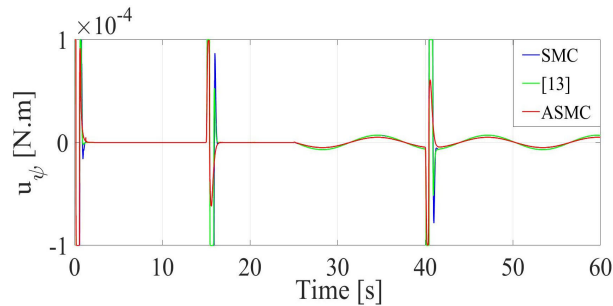

FIGURE 12. Control input signal u_θ.

FIGURE 13. Control input signal u_ψ.

FIGURE 14. Adaptation gain for altitude.

FIGURE 15. Adaptation gain for roll angle.
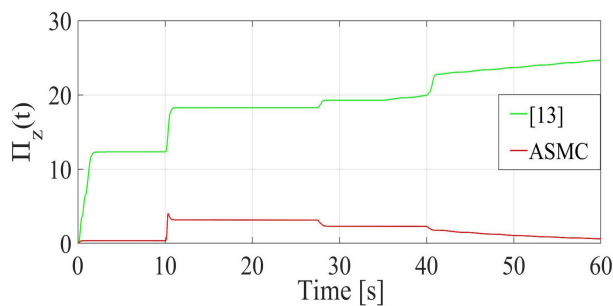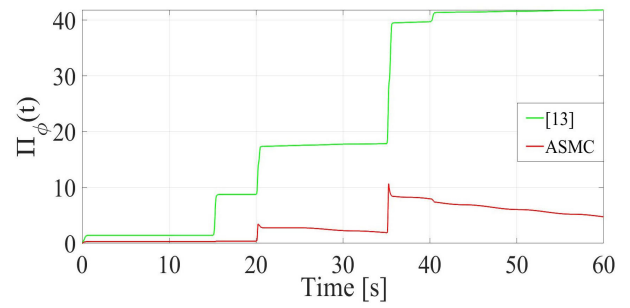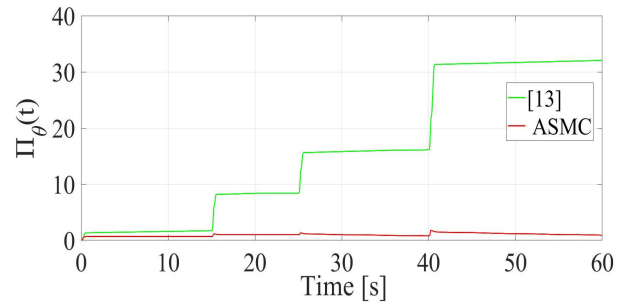

FIGURE 16. Adaptation gain for pitch angle.

FIGURE 17. Adaptation gain for yaw angle.

developed, comparing it with the one proposed in [13]. It is worth noting that the proposed algorithm exhibits effective adaptation to variations in the desired trajectory. Specifically, at the beginning, there is an amplification of the gain, which drives the sliding surface to converge in finite time.
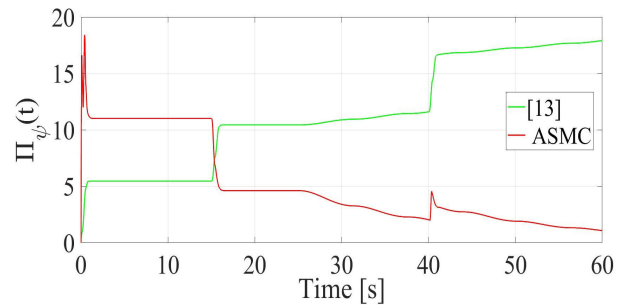
Once the ASMC reaches the objective, the gain amplitude converges toward zero. Now, based on the results of adaptive law proposed in [13], it can be seen that the gain curve increases as time passes, of which, every variation of the desired trajectory, results on the gain increasing, and at the moment that a disturbance is added, there is a divergence, causing the appearance of the chattering phenomenon in the control signals.

Remark 7: It should be mentioned that the adaptation law used in [13] has a weak adaptation with the dynamic system, where we can see in their results the amplification with time, and this is not our case where the proposed adaptation law has a good performance.

To effectively demonstrate the superiority of the proposed ASMC in comparison to the conventional SMC and algorithm presented in [13], a set of metrics to evaluate the energy control signal performance is used, such as the Control Signal Energy, $CSE = \sum_{i=1}^{N} u^2(i)T_s$, that measures the total
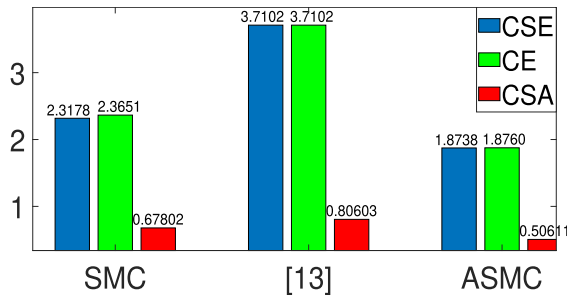
FIGURE 18. Energy performance metrics.

TABLE 4. Tracking error metrics.

Approach	Attitude		
	$\sum_{i=\phi}^{\psi} RMSE_i$	$\sum_{i=\phi}^{\psi} IAE_i$	$\sum_{i=\phi}^{\psi} ISE_i$
SMC	0.0678	70.2531	8.5805
[13]	0.1071	78.9166	10.7315
ASMC	0.0425	31.4808	4.2331
	Altitude		
	RMSE	IAE	ISE
SMC	0.0072	4.8761	0.2179
[13]	0.0111	12.2090	0.5256
ASMC	0.0045	4.1315	0.0861

energy consumption, the Control Signal Amplitude, $CSA = \frac{1}{N} \sum_{i=1}^{N} |u(i)|$, that measures the average amplitude of the control signal and the Control effort, $CE = \int_0^T |u(t)| dt$, that measures effort expended by the controller to maintain or modify the system's behavior, where N is the total number of samples, T is the simulation time, and T_s is the sample time. In addition, a set of tracking error measures are examined to provide a quantitative measure to assess the accuracy of the proposed control strategy i.e., Root Mean Square Error, $RMSE = \sqrt{\frac{1}{N} \sum_{i=1}^{N} (e(i))^2}$, Integral Absolute Error, $IAE = \int_0^T |e(t)| dt$, and Integral Square Error, $ISE = \int_0^T (e(t))^2 dt$.

According to the data shown in Fig. 18, clearly, the proposed control method performs better than other methods in terms of the input signal metrics. In particular, the proposed method achieves a significant reduction in CSE, CE, and CSA. This demonstrates that in contrast to other methods, the ASMC efficiently reduces CE and enhances performance consistency. In general, these results validate the effectiveness of the proposed method and demonstrate its superiority over existing control methods. The tracking error measurements in Table 4 prove that the proposed method is more efficient than the other methods, as shown by the consistently lower error values for all metrics, which demonstrates the effectiveness of the controller in accurately tracking the desired trajectory.

B. EXPERIMENTAL RESULTS
The proposed ASMC was evaluated and tested by the altitude flight experiment, using the low cost Parrot Mambo
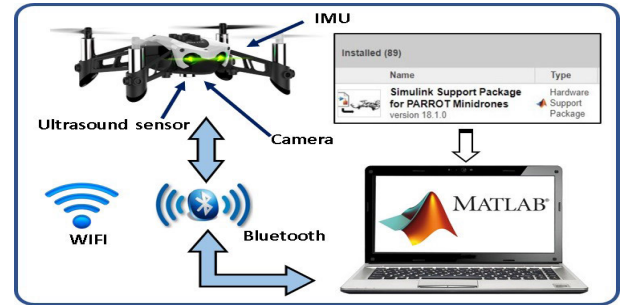

FIGURE 19. Control and connection of the Parrot Mambo Minidrone.

mini-drone type quadrotor, which is equipped with an inertial measurement unit (IMU) (3-axis accelerometer and 3-axis gyroscope), an ultrasonic sensor, and a camera with a resolution of 120×160 pixels and a refresh rate of 60 frames per second. The Parrot Mambo has the support package from Matlab/Simulink, that allows to get the internal sensor data and implement real-time control algorithms. The generated Matlab/Simulink code is deployed on the Parrot Mambo quadrotor via Bluetooth, as seen in Fig. 19. The sampling time of the flight algorithm is set to $T = 0.005sec$. The angular velocity, linear velocity, position and attitude of the mini-UAV are estimated via Kalman filter. The experimental test was conducted indoors on a surface area of $2m^2$ with a height of $3m$. Two different flight scenarios were designed to evaluate the proposed controller. The first scenario considers a fixed trajectory with a robustness test, the second, a variable reference trajectory.

1) SCENARIO 01 HOVERING
Here, the flight path is set for the quadcopter to rise vertically at $1.1m$, from the ground, then it hovers at this predefined altitude. Subsequently, a vertical force is applied to the CM, at the 20th and 32nd seconds, emulating an external disturbance of more than 20%. This experiment serves to test the control law robustness, to guarantee the path following in presence of external disturbances, demonstrating the evolution of the adaptation law. Fig. 20 shows the altitude trajectory of the drone, which reaches the desired altitude with a good settling time of $4s$ sec with a slight overshoot, and in the steady state ($10s < t < 20s$) the drone hovers around the desired value with high precision. Note, that when the external force is applied, the drone drop around 20 cm, but it returns quickly to the trajectory, which is proof of the robustness of the proposed ASMC.

The control signal, illustrated in Fig. 21 has two behaviours: 1) the trajectory before the perturbation, where the signal is within the saturation limits with a minimum of oscillations, 2) the trajectory after the perturbation, applying the external force, where it can be notice an amplification for $20s < t < 35s$ of the signal with oscillation, but having a short saturation, that is caused by the response of the ASMC to the amplitude of the two applied forces that move the vehicle $20cm$ below of the desired altitude.
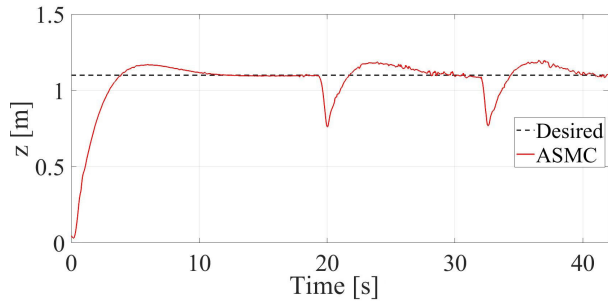
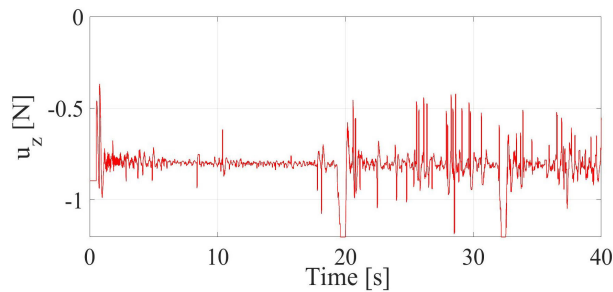**FIGURE 20.** Altitude trajectory tracking response against disturbances.

FIGURE 21. Control input signal u_z (scenario 01).

FIGURE 22. Adaptation gain (scenario 01).

FIGURE 23. Experimental environment.

FIGURE 24. Altitude tracking trajectory response.
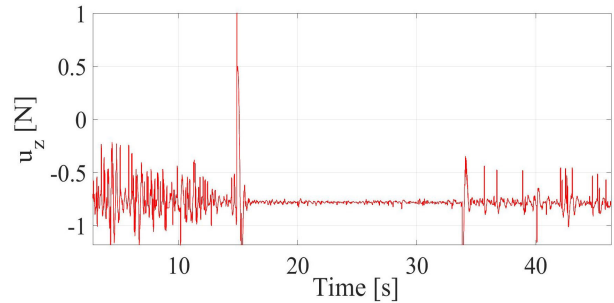
FIGURE 25. Control input signal u_z (scenario 02).
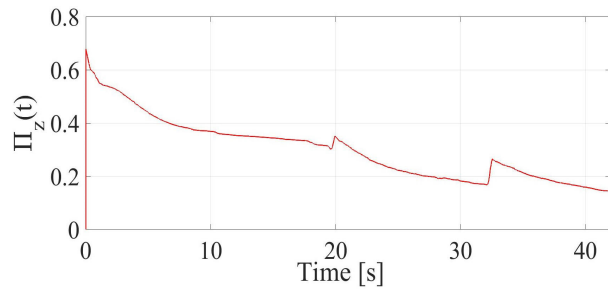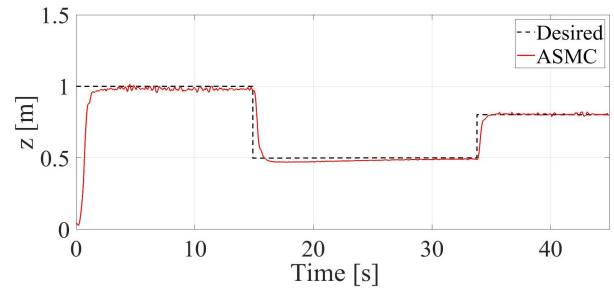

FIGURE 26. Adaptation gain (scenario 02).

Fig. 22 illustrates the adaptive law evolution. It is clear that the it fits perfectly with the time; at the beginning, the parameter are increased to reach the desired trajectory. Once the drone arrives at the reference, the parameter decreases slightly to avoid an amplification of the control signal, preventing a loss of energy by the phenomenon of chattering. Notice two increases at $t = 20s$ and $t = 32s$, due to the added external force, indicating that the adaptive law works perfectly also in the presence of an external perturbation.

2) SCENARIO 02 TRAJECTORY TRACKING
To evaluate the controller effectiveness, a trajectory tracking task is applied, with the reference similar to the one in the simulation, as shown in the snap shop sequence of Fig. 23 for different desired values of altitude $z_d = [1\ 0.5\ 0.8]m$, with initial condition, $z_0 = 0$.

Fig. 24 shows the trajectory in altitude, where the drone can track the desired altitude with a good transient phase and
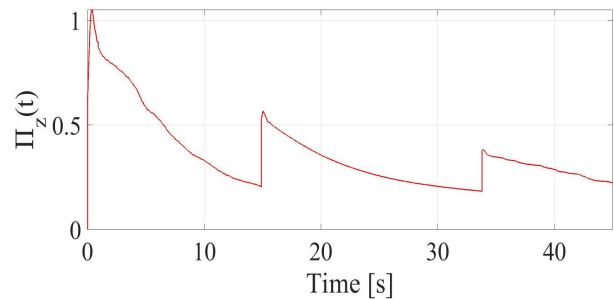
low settling time without overshoots; it can also follow the flight path with high precision in the steady-state phase.

Control signal u_z is shown in Fig. 25, it satisfies the saturation limits with a few oscillations when flying at the first desired value of $1m$, while during the second and third desired values (0.5m and 0.8m), the control signal is smooth,

and the control law guarantees a high performance trajectory tracking. Fig. 26 displays the course of the adaptation law. As in the first scenario, the parameter is increased to reach the required trajectory. Once the drone achieves the altitude reference, the parameter descend; we also notice two rises at $t = 15s$ and $t = 32s$, which is due to the shift of the trajectory for both accelerating the tracking and enhancing the performance of each transient regime. Afterward, the adaptation law works excellently for the tasks of trajectory tracking.

Remark 8: The saturation's effect in ($t \in \{15, 34\}sec$) can be justified by the trajectory choice because, at this moment, there is an abrupt change of the flight path; however, the stability is still well guaranteed.

VI. CONCLUSION

This paper proposes a new ASMC for quadrotor trajectory tracking control. This purpose has been achieved by considering different conditions; in the presence of external disturbances, parametric uncertainties with an unknown upper bound, and input saturation. The proposed control architecture is based on adaptive sliding mode control; by developing an adaptation law that gives the advantage of handling unknown uncertainties with a gain that has no overestimation and leads to convergence in a finite time. Secondly, we treated the input saturation constraint via the integration of an auxiliary system. The stability analysis performed through Lyapunov theory; shows the boundedness of all signals of the closed-loop system using the proposed control law and ensures the convergence in finite-time of the tracking errors. Simulations have been performed including a comparative study between the proposed control law and a classical SMC and a recent approach reported in the literature. We also employed a performance criteria method, showing the superiority and efficiency of the proposed controller in handling disturbances with an unknown upper bound with less effort. In addition, the proposed controller has been evaluated in the presence of actuator constraints specific to the Parrot Mambo quadrotor, which is known to have limited thrust capabilities. To further test the robustness of the control strategy, an external disturbance has been added during the experiments, simulating the effect of wind gusts on the quadrotor's motion. Despite these challenging conditions, the obtained results highlight the potential of the proposed controller for real-world applications where disturbances and hardware limitations are common challenges to overcome.

REFERENCES

[1] M. Idrissi, M. Salami, and F. Annaz, "A review of quadrotor unmanned aerial vehicles: Applications, architectural design and control algorithms," *J. Intell. Robotic Syst.*, vol. 104, no. 2, pp. 1–33, Feb. 2022.

[2] T. Zubowicz, K. Arminski, and A. Kusalewicz, "Quadrotor flight controller design using classical tools," *Int. J. Control, Autom. Syst.*, vol. 18, no. 3, pp. 730–738, Mar. 2020.

[3] L. Liu, M. Chen, and T. Li, "Disturbance observer-based LQR tracking control for unmanned autonomous helicopter slung-load system," *Int. J. Control, Autom. Syst.*, vol. 20, no. 4, pp. 1166–1178, Apr. 2022.

[4] V. P. Shankaran, S. I. Azid, U. Mehta, and A. Fagiolini, "Improved performance in quadrotor trajectory tracking using MIMO PI$^\lambda$-D control," *IEEE Access*, vol. 10, pp. 110646–110660, 2022.

[5] X. Lyu, J. Zhou, H. Gu, Z. Li, S. Shen, and F. Zhang, "Disturbance observer based hovering control of quadrotor tail-sitter VTOL UAVs using H$_\infty$ synthesis," *IEEE Robot. Autom. Lett.*, vol. 3, no. 4, pp. 2910–2917, Oct. 2018.

[6] H. E. Glida, L. Abdou, A. Chelihi, C. Sentouh, and S.-E.-I. Hasseni, "Optimal model-free backstepping control for a quadrotor helicopter," *Nonlinear Dyn.*, vol. 100, pp. 3449–3468, Jun. 2020.

[7] H. Wang, N. Li, Y. Wang, and B. Su, "Backstepping sliding mode trajectory tracking via extended state observer for quadrotors with wind disturbance," *Int. J. Control, Autom. Syst.*, vol. 19, no. 10, pp. 3273–3284, Oct. 2021.

[8] T. Jiang, T. Song, and D. Lin, "Integral sliding mode based control for quadrotors with disturbances: Simulations and experiments," *Int. J. Control, Autom. Syst.*, vol. 17, no. 8, pp. 1987–1998, Aug. 2019.

[9] N. Fethalla, M. Saad, H. Michalska, and J. Ghommam, "Robust observer-based dynamic sliding mode controller for a quadrotor UAV," *IEEE Access*, vol. 6, pp. 45846–45859, 2018.

[10] M. E. Antonio-Toledo, E. N. Sanchez, A. Y. Alanis, J. A. Flórez, and M. A. Perez-Cisneros, "Real-time integral backstepping with sliding mode control for a quadrotor UAV," *IFAC-PapersOnLine*, vol. 51, no. 13, pp. 549–554, 2018.

[11] F. Qiao, J. Shi, X. Qu, and Y. Lyu, "Adaptive back-stepping neural control for an embedded and tiltable V-tail morphing aircraft," *Int. J. Control, Autom. Syst.*, vol. 20, no. 2, pp. 678–690, Feb. 2022.

[12] T. Huang, D. Huang, Z. Wang, X. Dai, and A. Shah, "Generic adaptive sliding mode control for a quadrotor UAV system subject to severe parametric uncertainties and fully unknown external disturbance," *Int. J. Control, Autom. Syst.*, vol. 19, no. 2, pp. 698–711, Feb. 2021.

[13] M. Labbadi and M. Cherkaoui, "Robust adaptive backstepping fast terminal sliding mode controller for uncertain quadrotor UAV," *Aerosp. Sci. Technol.*, vol. 93, Oct. 2019, Art. no. 105306.

[14] M. Labbadi and M. Cherkaoui, "Robust adaptive global time-varying sliding-mode control for finite-time tracker design of quadrotor drone subjected to Gaussian random parametric uncertainties and disturbances," *Int. J. Control, Autom. Syst.*, vol. 19, no. 6, pp. 2213–2223, Jun. 2021.

[15] C. Zhang, T. Chen, W. Shang, Z. Zheng, and H. Yuan, "Adaptive super-twisting distributed formation control of multi-quadrotor under external disturbance," *IEEE Access*, vol. 9, pp. 148104–148117, 2021.

[16] W. Zeng, L. Zheng, M. Chen, Y. Lin, G. Wang, B. Gao, and S. Huang, "A generalized multivariable adaptive super-twisting control and observation for amphibious robot," *IEEE Access*, vol. 10, pp. 129588–129598, 2022.

[17] G. Shen, Y. Xia, J. Zhang, and B. Cui, "Adaptive super-twisting sliding mode altitude trajectory tracking control for reentry vehicle," *ISA Trans.*, vol. 132, pp. 329–337, Jan. 2023.

[18] M. Labbadi, M. Defoort, G. P. Incremona, and M. Djemai, "Fractional-order integral terminal sliding-mode control for perturbed nonlinear systems with application to quadrotors," *Int. J. Robust Nonlinear Control*, Jan. 2023.

[19] J. Wang, K. A. Alattas, Y. Bouteraa, O. Mofid, and S. Mobayen, "Adaptive finite-time backstepping control tracker for quadrotor UAV with model uncertainty and external disturbance," *Aerosp. Sci. Technol.*, vol. 133, Feb. 2023, Art. no. 108088.

[20] S. Larguech, S. Aloui, O. Pagès, A. El Hajjaji, and A. Chaari, "Robust adaptive controller for the diesel engine air path with input saturation," *Int. J. Control, Autom. Syst.*, vol. 17, no. 10, pp. 2541–2549, Oct. 2019.

[21] K. Eliker, S. Grouni, M. Tadjine, and W. Zhang, "Practical finite time adaptive robust flight control system for quad-copter UAVs," *Aerosp. Sci. Technol.*, vol. 98, Mar. 2020, Art. no. 105708.

[22] K. Liu, R. Wang, X. Wang, and X. Wang, "Anti-saturation adaptive finite-time neural network based fault-tolerant tracking control for a quadrotor UAV with external disturbances," *Aerosp. Sci. Technol.*, vol. 115, Aug. 2021, Art. no. 106790.

[23] N. Cao and A. F. Lynch, "Inner-outer loop control for quadrotor UAVs with input and state constraints," *IEEE Trans. Control Syst. Technol.*, vol. 24, no. 5, pp. 1797–1804, Sep. 2016.

[24] V. Utkin, "Variable structure systems with sliding modes," *IEEE Trans. Autom. Control*, vol. AC-22, no. 2, pp. 212–222, Apr. 1977.

[25] R. Xu and Ü. Özguner, "Sliding mode control of a class of underactuated systems," *Automatica*, vol. 44, no. 1, pp. 233–241, Jan. 2008.

[26] F. Muñoz, E. S. Espinoza, I. González-Hernández, S. Salazar, and R. Lozano, "Robust trajectory tracking for unmanned aircraft systems using a nonsingular terminal modified super-twisting sliding mode controller," *J. Intell. Robotic Syst.*, vol. 93, nos. 1–2, pp. 55–72, Feb. 2019.

[27] M. Pouzesh and S. Mobayen, "Event-triggered fractional-order sliding mode control technique for stabilization of disturbed quadrotor unmanned aerial vehicles," *Aerosp. Sci. Technol.*, vol. 121, Feb. 2022, Art. no. 107337.

[28] Q. Xu, Z. Wang, and Z. Zhen, "Adaptive neural network finite time control for quadrotor UAV with unknown input saturation," *Nonlinear Dyn.*, vol. 98, no. 3, pp. 1973–1998, Nov. 2019.

[29] J. Zhang, Z. Ren, C. Deng, and B. Wen, "Adaptive fuzzy global sliding mode control for trajectory tracking of quadrotor UAVs," *Nonlinear Dyn.*, vol. 97, no. 1, pp. 609–627, Jul. 2019.

[30] X. Lin, Y. Wang, and Y. Liu, "Neural-network-based robust terminal sliding-mode control of quadrotor," *Asian J. Control*, vol. 24, no. 1, pp. 427–438, Jan. 2022.

[31] S. Laghrouche, M. Harmouche, Y. Chitour, H. Obeid, and L. M. Fridman, "Barrier function-based adaptive higher order sliding mode controllers," *Automatica*, vol. 123, Jan. 2021, Art. no. 109355.

[32] J. A. Moreno, D. Y. Negrete, V. Torres-González, and L. Fridman, "Adaptive continuous twisting algorithm," *Int. J. Control*, vol. 89, no. 9, pp. 1798–1806, Sep. 2016.

[33] G. P. Incremona, M. Cucuzzella, and A. Ferrara, "Adaptive suboptimal second-order sliding mode control for microgrids," *Int. J. Control*, vol. 89, no. 9, pp. 1849–1867, Sep. 2016.

[34] T. R. Oliveira, J. P. V. Cunha, and L. Hsu, "Adaptive sliding mode control based on the extended equivalent control concept for disturbances with unknown bounds," in *Advances in Variable Structure Systems and Sliding Mode Control-Theory and Applications*. Berlin, Germany: Springer, 2018, pp. 149–163.

[35] C. Edwards and Y. B. Shtessel, "Adaptive continuous higher order sliding mode control," *Automatica*, vol. 65, pp. 183–190, Mar. 2016.

[36] G. Bartolini, A. Levant, F. Plestan, M. Taleb, and E. Punta, "Adaptation of sliding modes," *IMA J. Math. Control Inf.*, vol. 30, no. 3, pp. 285–300, Sep. 2013.

[37] Y. B. Shtessel, J. A. Moreno, and L. M. Fridman, "Twisting sliding mode control with adaptation: Lyapunov design, methodology and application," *Automatica*, vol. 75, pp. 229–235, Jan. 2017.

[38] M. Labbadi, Y. Boukal, and M. Cherkaoui, "Path following control of quadrotor UAV with continuous fractional-order super twisting sliding mode," *J. Intell. Robotic Syst.*, vol. 100, nos. 3–4, pp. 1429–1451, Dec. 2020.

[39] F. Muñoz, I. González-Hernández, S. Salazar, E. S. Espinoza, and R. Lozano, "Second order sliding mode controllers for altitude control of a quadrotor UAS: Real-time implementation in outdoor environments," *Neurocomputing*, vol. 233, pp. 61–71, Apr. 2017.

[40] O. Mechali, L. Xu, X. Xie, and J. Iqbal, "Fixed-time nonlinear homogeneous sliding mode approach for robust tracking control of multirotor aircraft: Experimental validation," *J. Franklin Inst.*, vol. 359, no. 5, pp. 1971–2029, Mar. 2022.

[41] X. Shao, G. Sun, W. Yao, J. Liu, and L. Wu, "Adaptive sliding mode control for quadrotor UAVs with input saturation," *IEEE/ASME Trans. Mechatronics*, vol. 27, no. 3, pp. 1498–1509, Jun. 2022.

[42] K. Mei, S. Ding, and X. Yu, "A generalized supertwisting algorithm," *IEEE Trans. Cybern.*, vol. 53, no. 6, pp. 3951–3960, Jun. 2023.

[43] Z. Zhao, D. Cao, J. Yang, and H. Wang, "High-order sliding mode observer-based trajectory tracking control for a quadrotor UAV with uncertain dynamics," *Nonlinear Dyn.*, vol. 102, no. 4, pp. 2583–2596, Dec. 2020.

[44] W. Liu, X. Cheng, and J. Zhang, "Command filter-based adaptive fuzzy integral backstepping control for quadrotor UAV with input saturation," *J. Franklin Inst.*, vol. 360, no. 1, pp. 484–507, Jan. 2023.

[45] Y. Huang, Z. Zheng, L. Sun, and M. Zhu, "Saturated adaptive sliding mode control for autonomous vessel landing of a quadrotor," *IET Control Theory Appl.*, vol. 12, no. 13, pp. 1830–1842, Sep. 2018.

[46] C. An, S. Jia, J. Zhou, and C. Wang, "Fast model-free learning for controlling a quadrotor UAV with designed error trajectory," *IEEE Access*, vol. 10, pp. 79669–79680, 2022.

[47] Z. Chang, H. Chu, and Y. Shao, "Quadrotor trajectory-tracking control with actuator saturation," *Electronics*, vol. 12, no. 3, p. 484, Jan. 2023.

[48] H. Karami, K. A. Alattas, S. Mobayen, and A. Fekih, "Adaptive integral-type terminal sliding mode tracker based on active disturbance rejection for uncertain nonlinear robotic systems with input saturation," *IEEE Access*, vol. 9, pp. 129528–129538, 2021.

[49] Y. Zhao, X. Sun, G. Wang, and Y. Fan, "Adaptive backstepping sliding mode tracking control for underactuated unmanned surface vehicle with disturbances and input saturation," *IEEE Access*, vol. 9, pp. 1304–1312, 2021.

[50] L. Chen, Z. Liu, H. Gao, and G. Wang, "Robust adaptive recursive sliding mode attitude control for a quadrotor with unknown disturbances," *ISA Trans.*, vol. 122, pp. 114–125, Mar. 2022.

[51] K. W. X. Zhang and Y. Lu, "Modelling and identification of quadrotor robot," *Abstract Appl. Anal.*, vol. 2014, no. 1, pp. 1–6, 2012.

[52] B. L. Stevens and F. L. Lewis, *Aircraft Control and Simulation*. Hoboken, NJ, USA: Wiley, 2003.

[53] B. Etkin and L. D. Reid, *Dynamics of Flight: Stability and Control*. Hoboken, NJ, USA: Wiley, 1996.

[54] C. Wen, J. Zhou, Z. Liu, and H. Su, "Robust adaptive control of uncertain nonlinear systems in the presence of input saturation and external disturbance," *IEEE Trans. Autom. Control*, vol. 56, no. 7, pp. 1672–1678, Jul. 2011.

[55] J. Sun, J. Yi, and Z. Pu, "Fixed-time adaptive fuzzy control for uncertain nonstrict-feedback systems with time-varying constraints and input saturations," *IEEE Trans. Fuzzy Syst.*, vol. 30, no. 4, pp. 1114–1128, Apr. 2022.

[56] M. Wang, L. Huang, and C. Yang, "NN-based adaptive tracking control of discrete-time nonlinear systems with actuator saturation and event-triggering protocol," *IEEE Trans. Syst., Man, Cybern. Syst.*, vol. 51, no. 12, pp. 7613–7621, Dec. 2021.

[57] M. Krstic and A. Smyshlyaev, *Boundary Control of PDEs: A Course on Backstepping Designs*. Philadelphia, PA, USA: SIAM, 2008.

[58] X. Huang, W. Lin, and B. Yang, "Global finite-time stabilization of a class of uncertain nonlinear systems," *Automatica*, vol. 41, no. 5, pp. 881–888, May 2005.

[59] S. P. Bhat and D. S. Bernstein, "Finite-time stability of continuous autonomous systems," *SIAM J. Control Optim.*, vol. 38, no. 3, pp. 751–766, Jan. 2000.

[60] S. Yu, X. Yu, B. Shirinzadeh, and Z. Man, "Continuous finite-time control for robotic manipulators with terminal sliding mode," *Automatica*, vol. 41, no. 11, pp. 1957–1964, Nov. 2005.

[61] J. Yu, P. Shi, and L. Zhao, "Finite-time command filtered backstepping control for a class of nonlinear systems," *Automatica*, vol. 92, pp. 173–180, Jun. 2018.

[62] H. K. Khalil, *Nonlinear Systems*, vol. 115, 3rd ed. Upper Saddle River, NJ, USA: Prentice-Hall, 2002.

[63] M. Chen, S. S. Ge, and B. Ren, "Adaptive tracking control of uncertain MIMO nonlinear systems with input constraints," *Automatica*, vol. 47, no. 3, pp. 452–465, Mar. 2011.

[64] H. Hassani, A. Mansouri, and A. Ahaitouf, "Robust autonomous flight for quadrotor UAV based on adaptive nonsingular fast terminal sliding mode control," *Int. J. Dyn. Control*, vol. 9, no. 2, pp. 619–635, Jun. 2021.

[65] O. Mofid and S. Mobayen, "Adaptive sliding mode control for finite-time stability of quad-rotor UAVs with parametric uncertainties," *ISA Trans.*, vol. 72, pp. 1–14, Jan. 2018.

[66] X. Huang, Y. Yan, and Z. Huang, "Finite-time control of underactuated spacecraft hovering," *Control Eng. Pract.*, vol. 68, pp. 46–62, Nov. 2017.

[67] K. Eliker, S. Grouni, M. Tadjine, and W. Zhang, "Quadcopter nonsingular finite-time adaptive robust saturated command-filtered control system under the presence of uncertainties and input saturation," *Nonlinear Dyn.*, vol. 104, no. 2, pp. 1363–1387, Apr. 2021.

KHELIL SIDI BRAHIM received the master's degree in automatic control from the University of Biskra, Algeria, in 2017. He is currently pursuing the Ph.D. degree in automatic control with the Modeling Information Systems Laboratory (MIS Lab), University of Picardie Jules Verne (UPJV), and the Modeling of Energetic Systems Laboratory (LMSE Lab), University of Biskra. His research interests include adaptive and robust control, UAV systems, sliding mode control, and trajectory tracking control.

AHMED EL HAJJAJI received the Ph.D. degree in automatic control and the H.D.R. degree from the University of Picardie Jules Verne (UPJV), France, in 1993 and 2000, respectively. He is currently a Full Professor and the Head of the Automatic Control and Vehicle Research Group, Modeling Information Systems Laboratory (MIS Lab), UPJV. He was the Director of the Professional Institute of Electrical Engineering and Industrial Computing from 2006 to 2012. Since 1994, he has published more than 350 journal and conference papers in the areas of advanced fuzzy control, fault detection, and diagnosis and fault tolerant control and their applications to vehicle dynamics, engine control, power systems, renewable energy conversion systems, and industrial processes. His research interests include fuzzy control, vehicle dynamics, fault-tolerant control, neural networks, maglev systems, and renewable energy conversion systems.

DAVID LARA ALABAZARES received the B.S. degree in electronic engineering from TecNM, Madero, Mexico, in 1996, the M.Sc. degree in automatic control from the Autonomous University of Tamaulipas, in 2001, and the Ph.D. degree in information and systems technologies from the University of Technology of Compiègne, France, in 2007. He is currently a Research Professor with TecNM, Misantla. His research interests include modeling and control of mechatronic systems, and renewable sustainable technology.

• • •

NADJIBA TERKI received the Engineering Diploma degree in automatics, the Magister Diploma degree in non-destructive control, and the Ph.D. degree in signal processing from Badji Mokhtar University, Annaba, Algeria, in 1994, 2000, and 2009, respectively. She currently serves as a Full Professor with the Electrical Engineering Department, Mohamed Khider University of Biskra, Algeria. Her research interests include digital signal and image processing, artificial intelligence, wavelet transform, and robust control.